Article

Cell Reports

PLEKHA4/*kramer* Attenuates Dishevelled Ubiquitination to Modulate Wnt and Planar Cell Polarity Signaling

Graphical Abstract

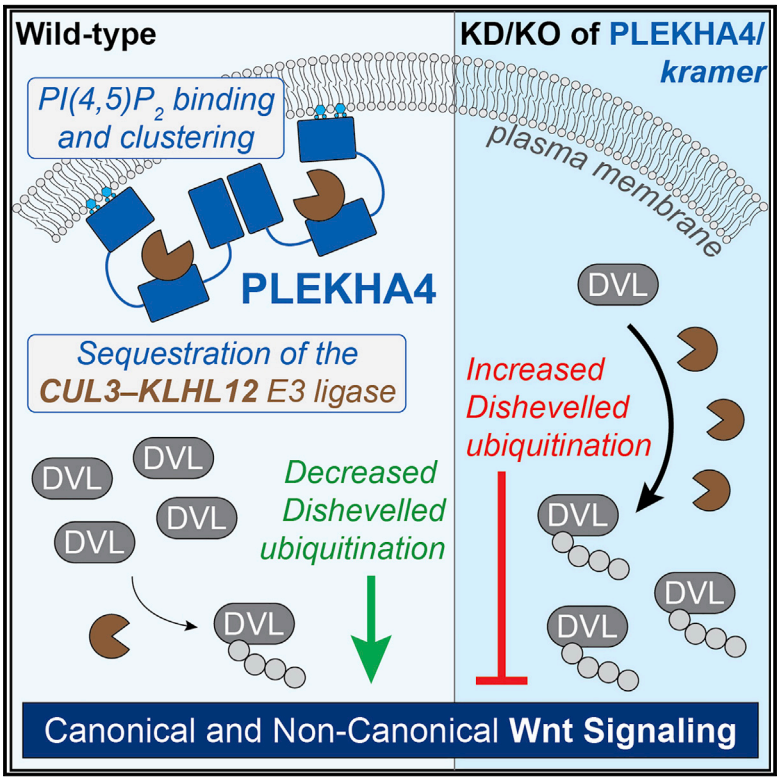

Authors

Adnan Shami Shah, Alex G. Batrouni, Dongsung Kim, ..., Michael L. Goldberg, Marcus B. Smolka, Jeremy M. Baskin

Correspondence

jeremy.baskin@cornell.edu

In Brief

Regulation of Wnt signaling is critical to metazoan development. Shami Shah et al. identify a phosphoinositide-binding protein, PLEKHA4/*kramer*, that enhances Wnt signaling in mammalian cells and the non-canonical pathway, planar cell polarity, in *Drosophila*. Mechanistically, PLEKHA4 sequesters the Cullin-3 E3 ligase adaptor KLHL12 in plasma membrane clusters, preventing Dishevelled polyubiquitination.

Highlights

- PLEKHA4 promotes Wnt signaling by inhibiting the degradation of Dishevelled (DVL)
- PLEKHA4 binds to PI(4,5)P_2 and oligomerizes into plasma membrane clusters
- The clusters sequester a Cullin-3 adaptor, KLHL12, preventing DVL ubiquitination
- The *Drosophila* PLEKHA4 homolog, *kramer*, regulates planar cell polarity signaling

Shami Shah et al., 2019, Cell Reports *27*, 2157–2170
May 14, 2019
https://doi.org/10.1016/j.celrep.2019.04.060

CellPress

Cell Reports
Article

PLEKHA4/*kramer* Attenuates Dishevelled Ubiquitination to Modulate Wnt and Planar Cell Polarity Signaling

Adnan Shami Shah,[1,2] Alex G. Batrouni,[1,2] Dongsung Kim,[2,3] Amith Punyala,[1,2] Wendy Cao,[1,2] Chun Han,[2,3] Michael L. Goldberg,[3] Marcus B. Smolka,[2,3] and Jeremy M. Baskin[1,2,4,*]
[1]Department of Chemistry and Chemical Biology, Cornell University, Ithaca, NY 14853, USA
[2]Weill Institute for Cell and Molecular Biology, Cornell University, Ithaca, NY 14853, USA
[3]Department of Molecular Biology and Genetics, Cornell University, Ithaca, NY 14853, USA
[4]Lead Contact
*Correspondence: jeremy.baskin@cornell.edu
https://doi.org/10.1016/j.celrep.2019.04.060

SUMMARY

Wnt signaling pathways direct key physiological decisions in development. Here, we establish a role for a pleckstrin homology domain-containing protein, PLEKHA4, as a modulator of signaling strength in Wnt-receiving cells. PLEKHA4 oligomerizes into clusters at PI(4,5)P_2-rich regions of the plasma membrane and recruits the Cullin-3 (CUL3) E3 ubiquitin ligase substrate adaptor Kelch-like protein 12 (KLHL12) to these assemblies. This recruitment decreases CUL3-KLHL12-mediated polyubiquitination of Dishevelled, a central intermediate in canonical and non-canonical Wnt signaling. Knockdown of PLEKHA4 in mammalian cells demonstrates that PLEKHA4 positively regulates canonical and non-canonical Wnt signaling via these effects on the Dishevelled polyubiquitination machinery. *In vivo* knockout of the *Drosophila melanogaster* PLEKHA4 homolog, *kramer*, selectively affects the non-canonical, planar cell polarity (PCP) signaling pathway. We propose that PLEKHA4 tunes the sensitivities of cells toward the stimulation of Wnt or PCP signaling by sequestering a key E3 ligase adaptor controlling Dishevelled polyubiquitination within PI(4,5)P_2-rich plasma membrane clusters.

INTRODUCTION

Wnt signaling controls key cell fate decisions in the development of multicellular eukaryotes, and its dysregulation can cause many human diseases (Clevers and Nusse, 2012). As such, Wnt signaling is subject to many points and types of regulation, both in cells that produce and in those that receive the secreted Wnt signals. In the Wnt-receiving cell, the engagement of Wnt proteins by the Frizzled family of cell-surface receptors (Janda et al., 2012) can activate different intracellular signaling pathways, including the canonical, β-catenin-dependent pathway and the non-canonical planar cell polarity (PCP) and Wnt-Ca^{2+} routes (Cadigan and Peifer, 2009; Devenport, 2014; Gómez-Orte et al., 2013; MacDonald et al., 2009; Wallingford, 2012).

A feature common to all Wnt signaling pathways is the involvement of the cytoplasmic protein Dishevelled (DVL), whose recruitment to the plasma membrane upon Wnt binding to Frizzled initiates the intracellular signal transduction pathways. Because of this dynamic behavior, the DVL proteins represent key factors that Wnt-receiving cells can use to tune the strength of the Wnt signal (Gao and Chen, 2010; Mlodzik, 2016; Wallingford and Habas, 2005). DVL levels are modulated by ubiquitination (Angers et al., 2006; Ganner et al., 2009; Gao et al., 2010; Miyazaki et al., 2004; Sharma et al., 2012; Wei et al., 2012). In particular, the E3 ubiquitin ligase Cullin-3 (CUL3), in complex with one of its substrate adaptors, Kelch-like protein 12 (KLHL12), catalyzes the polyubiquitination of DVL3, leading to the proteasomal degradation of the latter (Angers et al., 2006). By lowering DVL3 levels, the CUL3-KLHL12 E3 ligase diminishes the strength of Wnt signaling. Given that cells must dynamically tune their Wnt ligand sensitivities to different physiological settings, a major unanswered question is how this activity of CUL3-KLHL12 toward DVL3 is regulated.

CUL3 interacts physiologically with adaptors other than KLHL12 (Dubiel et al., 2018) and, in complex with KLHL12, functions at intracellular locations that are distinct from the plasma membrane (Jin et al., 2012; Rondou et al., 2008). For example, at the endoplasmic reticulum, CUL3-KLHL12 mediates monoubiquitination of the COPII vesicle component SEC31 to facilitate the formation of enlarged COPII vesicles that transport large cargoes such as collagen to the Golgi complex; local bursts of calcium regulate this action of CUL3-KLHL12 via the calcium-binding adaptor proteins PEF1 and ALG2 (Jin et al., 2012; McGourty et al., 2016). It remains unknown how these distinct activities of CUL3-KLHL12 are regulated. What factors modulate the interaction of CUL3-KLHL12 with DVL3? Do such putative factors act analogously to how PEF1 and ALG2 regulate CUL3-KLHL12 activity at the endoplasmic reticulum (ER)? One possibility is that plasma membrane-localized factors control CUL3-KLHL12 activity toward DVL3 in this membrane, the site of DVL3 action in Wnt signaling.

Key signaling molecules at the plasma membrane are the phosphoinositides (PIPs) PI4P and PI(4,5)P_2, which function in part by recruiting soluble proteins to the plasma membrane and allosterically regulating their function (Balla, 2013; Hammond et al., 2012). The largest family of PIP-binding proteins in

humans consists of the ~250 proteins containing a pleckstrin homology (PH) domain (Lemmon, 2008). Although a small minority of PH domain-containing proteins are known to bind a specific PIP species and to elicit defined signaling outcomes (e.g., PH domains from AKT and BTK), the molecular properties and physiological functions of the vast majority of PH domain-containing proteins remain unknown (Hammond and Balla, 2015).

Here, we report that the uncharacterized protein PLEKHA4 (pleckstrin homology domain-containing family A, member 4) is a plasma membrane-localized signaling adaptor that regulates CUL3-KLHL12-mediated ubiquitination of DVL3 and thus tunes the strength of Wnt signaling. We find that PLEKHA4 molecules assemble at $PI(4,5)P_2$-rich regions of the plasma membrane via a unique combination of its lipid-binding, oligomerization, and intrinsically disordered domains. PLEKHA4 physically interacts with CUL3-KLHL12 to recruit the E3 ligase to these plasma membrane assemblies. This recruitment is accompanied by a decrease in CUL3-KLHL12 E3 ligase activity toward its substrate, DVL, whose site of action in both the canonical Wnt and PCP signaling pathways is the plasma membrane. Consequently, PLEKHA4 causes DVL to accumulate, upregulating Wnt signaling in cultured mammalian cells. A knockout of the *Drosophila* PLEKHA4 homolog, *kramer*, exhibits defects in PCP signaling, speaking to the physiological relevance of our *in vitro* findings. We thus propose PLEKHA4 as a key modulator of Wnt and PCP signaling pathways through its function as an adaptor that tunes CUL3-KLHL12 activity at the plasma membrane.

RESULTS

PLEKHA4 Localizes to the Plasma Membrane via Interactions with $PI(4,5)P_2$

Our interest in PLEKHA4 emerged from a motivation to understand the roles for phosphoinositides in directing signaling via the engagement of their head group by effector proteins bearing both PH domains and additional domains for mediating signaling. PH domain-containing proteins number ~250 in humans, and the majority have not been extensively characterized (Lemmon, 2007). In particular, the PH domain-containing protein PLEKHA4, also known as PEPP1, is part of a family that includes several mediators of intracellular signaling (e.g., FAPP1/2 [D'Angelo et al., 2007; Godi et al., 2004], TAPP1/2 [Li and Marshall, 2015], and PLEKHA7/Hadp1 [Shah et al., 2016]). Other than a single report suggesting that its PH domain binds to phosphatidylinositol 3-phosphate (PI3P) (Dowler et al., 2000) and a computational study predicting that its PH domain binds to phosphatidylinositol 3,4,5-trisphosphate ($PI(3,4,5)P_3$) (Jungmichel et al., 2014), PLEKHA4 is an unstudied protein with no known cellular functions. We thus set out to elucidate its molecular properties, subcellular localization, protein interaction partners, and cellular and physiological roles.

We began our studies of PLEKHA4 by examining the properties of the PH domain and how it influences the subcellular localization of the protein. We found that a fluorescent protein fusion to PLEKHA4 localized to the plasma membrane (Figure 1A). This result was surprising because protein-lipid overlay assays had previously suggested to other investigators that the PH domain of PLEKHA4 binds to PI3P, which localizes to endosomes and not to the plasma membrane (Dowler et al., 2000; Schink et al., 2013).

We revisited the PIP binding of the PLEKHA4 PH domain (residues 45–167) using liposome sedimentation assays that assess protein-lipid interactions in the context of intact lipid bilayers, which represent a more physiologically relevant environment (Zhao and Lappalainen, 2012). The PLEKHA4 PH domain partially co-sedimented with liposomes containing any one of the three bis-phosphorylated PIPs ($PI(3,4)P_2$, $PI(3,5)P_2$, and $PI(4,5)P_2$) and exhibited little affinity for PI3P or the other PIP species (Figure 1B). Although moderate, the observed binding was specific, as it was abolished by the mutation of either of two key Arg residues in the PH domain predicted by a crystal structure to contact the PIP head group (Milburn et al., 2004) (Figures 1C and S1A).

A GFP-tagged PH domain adopted a diffuse cytosolic localization, suggesting that a monomeric PH domain was not sufficient to confer the membrane targeting of PLEKHA4 (Figure 1D). We noticed that just upstream of the PH domain were two other motifs that could mediate membrane binding: a putative amphipathic helix (H, residues 28–41) and a basic peptide (BP, residues 42–50) (Figure S1A). The fusion of these motifs to the PH domain afforded a minimal construct ($PLEKHA4^{H\text{-}BP\text{-}PH}$, residues 28–167) that mediated both strong and specific co-sedimentation with $PI(4,5)P_2$-containing liposomes and localization to the plasma membrane within cells (Figures 1E and 1F). Either a single F40E mutation in the helix motif or a quadruple mutation of Arg/Lys residues within the basic peptide to Ala (4A) abolished binding to $PI(4,5)P_2$-containing liposomes and the plasma membrane localization of a GFP fusion to this minimal construct (Figures 1G, 1H, and S1A).

To further establish the requirement of $PI(4,5)P_2$ for the plasma membrane localization of the $PLEKHA4^{H\text{-}BP\text{-}PH}$ construct, we transiently depleted this lipid by the stimulation of cells expressing the M1 muscarinic receptor (M1R) with its ligand, oxotremorine M, to induce phospholipase C-mediated $PI(4,5)P_2$ hydrolysis (Falkenburger et al., 2010a, 2010b). The activation of M1R in HeLa cells expressing H-BP-PH caused shifts in localization of both a $PI(4,5)P_2$ reporter (PH domain of PLCδ1) and GFP-tagged $PLEKHA4^{H\text{-}BP\text{-}PH}$ from the plasma membrane to the cytosol (Figure S1B).

PLEKHA4 Assembles into Higher-Order Structures at the Plasma Membrane

The above data establish a sequence of three N-terminal motifs responsible for PLEKHA4 plasma membrane localization. However, full-length PLEKHA4 is not uniformly distributed at the plasma membrane but is instead strikingly localized to puncta visible by conventional confocal microscopy (Figure 1A) and superresolution structured illumination microscopy (SR-SIM) (Figure 2A). Thus, additional factors beyond the N-terminal $PI(4,5)P_2$-binding domains may control the localization and/or assembly of the full-length protein.

The PLEKHA4 puncta did not colocalize with the markers of established assemblies at the plasma membrane, including clathrin-coated pits, caveolae, or endoplasmic reticulum-plasma membrane contact sites (Figures S2A–S2C). We also observed

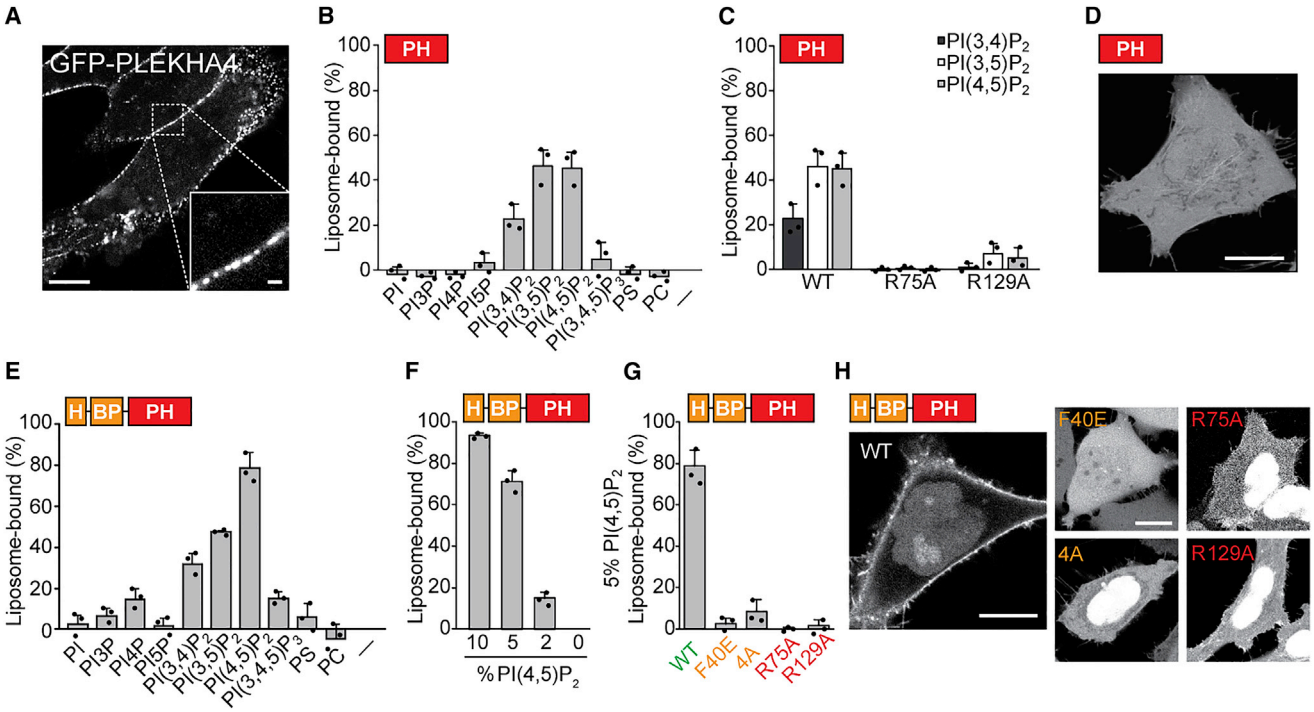

Figure 1. PLEKHA4 Localizes to the Plasma Membrane via Recognition of $PI(4,5)P_2$

(A) Confocal microscopy of HeLa cells transfected with GFP-PLEKHA4.

(B–G) Lipid-binding assays via co-sedimentation of PLEKHA4 domains with liposomes. Graphs show the percentage of the protein construct that co-sediments with an excess of liposome of defined composition. (B and C) Co-sedimentation of the wild-type mutants (B) or indicated point mutants (C) of the PLEKHA4 PH domain (amino acids 54–167) with liposomes, with 5% of the indicated PIP (or 20% of dioleoylphosphatidylserine [PS]) and the remainder as dioleoylphosphatidylcholine (PC) (n = 3). The (–) sign indicates no liposomes. (D) Confocal microscopy of HeLa cells transfected with a GFP-tagged PLEKHA4 PH domain (GFP-$PLEKHA4^{PH}$). (E–G) Co-sedimentation of wild-type constructs (E and F) or indicated point mutants (G) of a fusion of amphipathic helix, basic peptide, and PH domain ($PLEKHA4^{H\text{-}BP\text{-}PH}$, amino acids 28–167) with liposomes containing 5% of the indicated PIP (or 20% PS) and the remainder as PC (E), the indicated concentration of $PI(4,5)P_2$ (F), or 5% $PI(4,5)P_2$ (G) (n = 3).

(H) Confocal microscopy of wild-type or the indicated mutant of GFP-$PLEKHA4^{H\text{-}BP\text{-}PH}$. 4A refers to the quadruple mutant K42A/R43A/R48A/R49A. Scale bars: 10 μm (A [full size], D, and H); 1 μm (A [inset]).

See also Figure S1.

no colocalization with endosomal and lysosomal markers, which is consistent with our finding that the PH domain does not bind to PI3P (Figure S2D). We thus hypothesized that the puncta were the result of PLEKHA4 self-association. PLEKHA4 has two adjacent domains at the C terminus that could be responsible for the oligomerization into higher-order structures: a coiled-coil (CC) domain and an intrinsically disordered region (IDR).

Biochemical and imaging experiments support a role for both of these domains in the formation of the PLEKHA4 clusters. First, the isolated CC domain was cytoplasmically localized but could be recruited to the plasma membrane by co-overexpression with full-length PLEKHA4, suggesting a role in dimerization or higher-order oligomerization (Figure 2B). Second, a version of PLEKHA4 lacking the IDR remained at the plasma membrane but no longer assembled into puncta (Figure 2A). Third, a fusion of the CC and IDR domains formed large puncta in the cytoplasm that could, like the isolated CC domain, be recruited to the plasma membrane by full-length PLEKHA4 (Figure 2B). To complement these imaging data, we found via co-immunoprecipitation (co-IP) assays that both the isolated CC domain and a CC-IDR fusion could physically interact with full-length PLEKHA4 (Figure 2C).

The requirement of the IDR for puncta formation and the failure of full-length PLEKHA4 to colocalize with known organelle markers led us to hypothesize that the PLEKHA4 puncta may represent liquid-liquid phase-separated domains. Also referred to as membraneless organelles, these structures form via controlled aggregation of proteins and other biological molecules and can lead to their sequestration from the bulk cytosol (Hyman et al., 2014; Li et al., 2012; Mitrea and Kriwacki, 2016; Shin and Brangwynne, 2017). A recently recognized mechanism of phase separation in biological systems is via non-covalent interactions between highly unstructured, intrinsically disordered protein domains (Elbaum-Garfinkle et al., 2015; Lin et al., 2015; Nott et al., 2015).

To test whether the IDR of PLEKHA4 can mediate assembly into higher-order structures within cells, we deployed an optogenetic method that capitalizes on the propensity of the protein Cryptochrome-2 (CRY2) to homo-oligomerize upon exposure to blue light. By fusing a putative IDR to mCherry (mCh)-tagged CRY2, light can be used to trigger the formation of highly fluorescent, spherical cytoplasmic aggregates termed optoDroplets, whose presence indicates that the IDR can mediate cluster formation (Park et al., 2017; Shin et al., 2017).

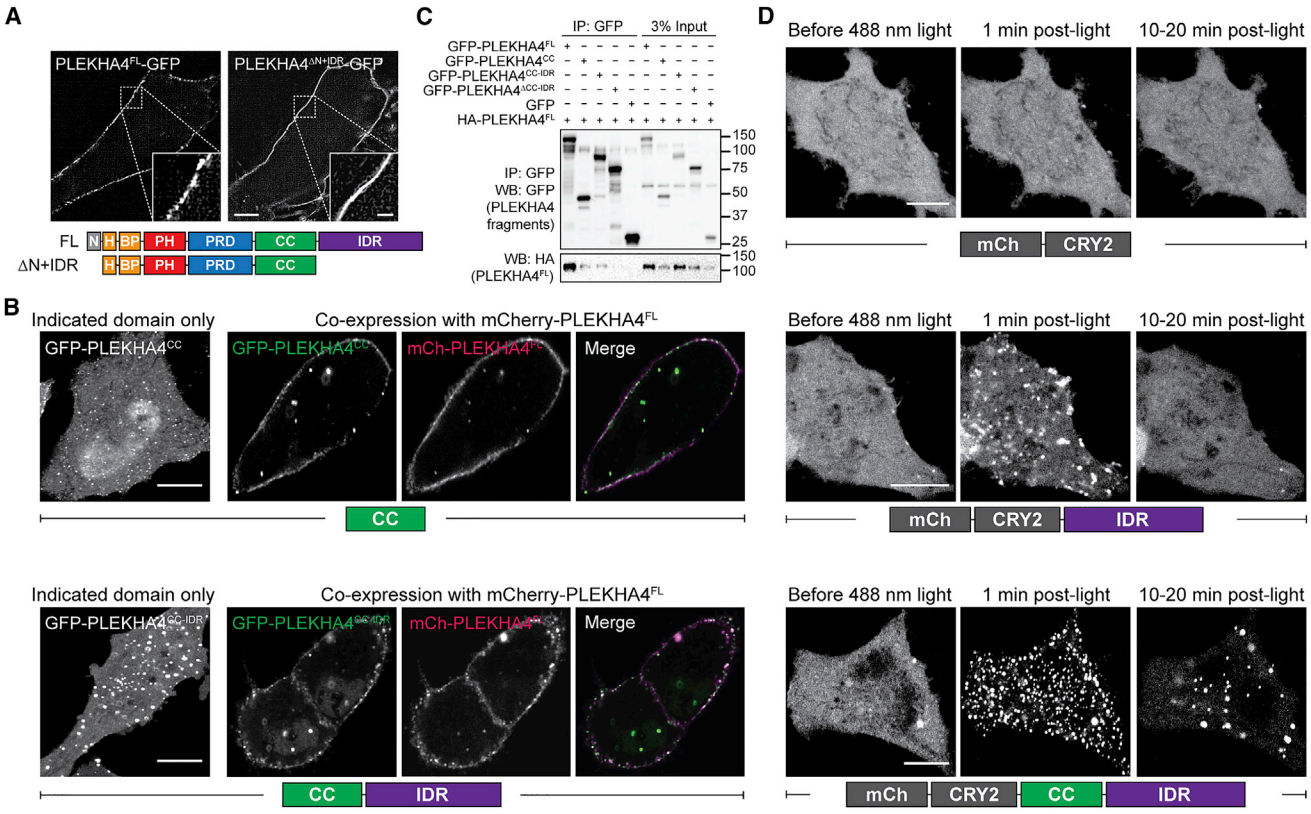

Figure 2. PLEKHA4 Oligomerizes into Clusters via Its Coiled-Coil and Intrinsically Disordered Regions

(A) Superresolution structured illumination microscopy (SR-SIM) of HeLa cells transfected with PLEKHA4^{FL}-GFP or PLEKHA4$^{\Delta IDR}$-GFP (amino acids 28–495).

(B) Confocal microscopy of HeLa cells transfected with a GFP-tagged PLEKHA4 coiled-coil domain construct (GFP-PLEKHA4^{CC}, amino acids 357–495), either alone or in combination with mCherry (mCh)-PLEKHA4^{FL} (top) or a GFP-tagged PLEKHA4 coiled-coil and intrinsically disordered region construct (GFP-PLEKHA4^{CC-IDR}, amino acids 357–779) alone or in combination with mCh-PLEKHA4^{FL} (bottom).

(C) Western blot analysis of anti-GFP immunoprecipitates of HeLa cells co-transfected with HA-PLEKHA4^{FL} and either the indicated GFP-PLEKHA4 fragment or GFP as a control.

(D) Relevant frames from time series (Videos S1, S2, and S3) of HeLa cells transfected with mCherry-CRY2, mCherry-CRY2-PLEKHA4^{IDR}, or mCherry-CRY2-PLEKHA4^{CC-IDR} subjected to brief photoactivation with a 488-nm pulse and monitored for the formation of reversible clusters or aggregates. Scale bars: 5 μm (A), 10 μm (B and D), and 1 μm (A, inset).

See also Figure S2.

We generated mCh-CRY2 fusion constructs to either the PLEKHA4 IDR or the CC-IDR domains. The exposure of cells expressing these domains to blue light led to the rapid formation of intensely fluorescent cytoplasmic aggregates (Figure 2D; Videos S1 and S2). Removal of blue light stimulation led to a partial disaggregation, indicating that cluster formation was reversible. As a negative control, the irradiation of cells expressing mCh-CRY2 under identical conditions did not lead to aggregate formation (Figure 2D; Video S3).

These results indicate that the C-terminal domains of PLEKHA4 are capable of assembly into higher-order structures in a cellular context. To further bolster the notion that avidity and cluster formation is a strong driving force for PLEKHA4 assembly at the plasma membrane, we note that transient PI(4,5)P_2 depletion did not cause a substantial shift in the localization of full-length GFP-PLEKHA4 (Figure S1C). Attempts to purify the isolated C-terminal domains or full-length protein for *in vitro* analysis were not successful, and a comprehensive *in vitro* characterization would be necessary to fully understand the nature of the plasma membrane PLEKHA4 puncta. Nevertheless, it is interesting to speculate that the PLEKHA4-positive puncta at the plasma membrane may represent oligomeric, liquid-liquid phase-separated clusters.

PLEKHA4 Associates with KLHL12, an Adaptor of the E3 Ubiquitin Ligase CUL3

To explore possible additional components of the PLEKHA4 puncta and to ascertain a function for these assemblies, we searched for the protein-protein interaction partners of PLEKHA4. We generated stable HEK293 cell lines expressing GFP-PLEKHA4 or, as a negative control, GFP, and performed stable isotope labeling by amino acids in cell culture (SILAC)-enabled quantitative proteomics (Hoedt et al., 2014) of anti-GFP immunoprecipitates from each of these cell lines (Figure 3A; Table S1). The strongest hit from these experiments was KLHL12.

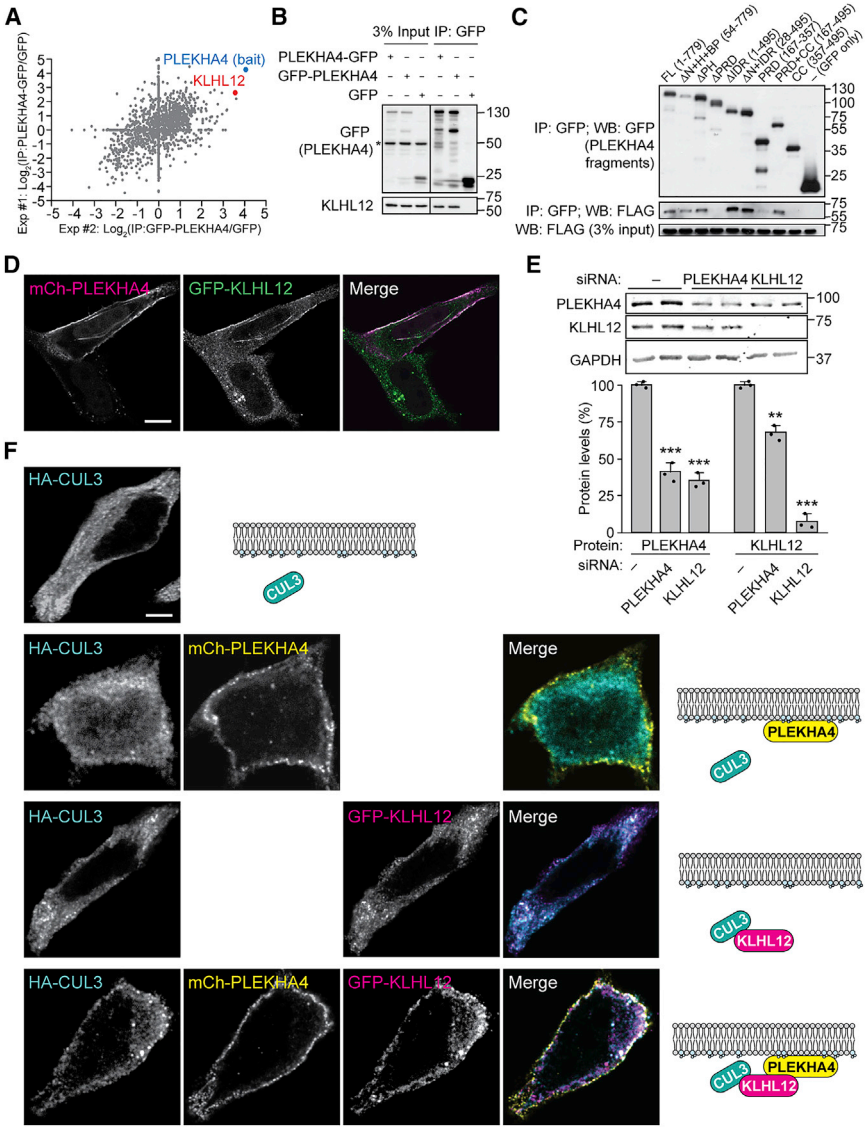

Figure 3. PLEKHA4 Associates with KLHL12, an Adaptor of the E3 Ubiquitin Ligase CUL3

(A) KLHL12 is an interactor of PLEKHA4. Scatterplot shows the enrichment of proteins present in anti-GFP immunoprecipitates from SILAC-labeled cells expressing GFP-PLEKHA4 or PLEKHA4-GFP compared to those expressing GFP only. The plot shows the correlation between two different experiments, one using PLEKHA4-GFP as the experimental bait (y axis) and one using GFP-PLEKHA4 as the bait (x axis). Proteins were identified by shotgun proteomics (see Table S1 for the full list of identified proteins).

(B and C) Western blot analysis of anti-GFP immunoprecipitates of HeLa cell lines that were transfected with GFP, GFP-PLEKHA4, or PLEKHA-GFP for the immunoprecipitation of endogenous KLHL12 (B) or transfected with 3xFLAG-KLHL12 and the indicated GFP-PLEKHA4 fragment (C). The asterisk indicates non-specific background immunoreactivity.

(D) Live-cell confocal microscopy of HeLa cells co-transfected with mCh-PLEKHA4 and GFP-KLHL12. Note that the top cell expresses both proteins, whereas the bottom cell expresses only GFP-KLHL12.

(E) Western blot analysis and quantification of lysates from HeLa cells treated with siRNA against PLEKHA4 or KLHL12 or a control siRNA (–). $^{**}p < 0.01$, $^{***}p < 0.001$ (n = 3).

(F) Immunofluorescence analysis of HeLa cells transfected with the indicated combination of HA-CUL3 (cyan), mCh-PLEKHA4 (yellow), and GFP-KLHL12 (magenta), with an illustration of the subcellular localizations at right. Scale bars: 10 μm.

We validated the interaction of both PLEKHA4-GFP and GFP-PLEKHA4 with endogenous KLHL12 by co-IP followed by western blot (Figure 3B). To map the interacting regions, we performed co-IP of KLHL12 with several PLEKHA4 truncations and isolated domains (Figure 3C). The minimal region that interacted with KLHL12 is the Pro-rich domain (PRD) of PLEKHA4. A construct including both the PRD and the CC domains (PLEKHA4^{PRD-CC}) exhibited a much stronger interaction with KLHL12, which we attribute to the capacity of PLEKHA4^{PRD-CC} to oligomerize.

We found that PLEKHA4 can control KLHL12 localization in cells. Whereas fluorescently tagged KLHL12 localizes to cytoplasmic puncta, consistent with previous studies (Mai et al., 2004) (Figure 3D, bottom cell), co-overexpression of PLEKHA4 with KLHL12 recruited KLHL12 to the plasma membrane (Figure 3D, top cell). Loss-of-function studies provide further evidence of a PLEKHA4-KLHL12 interaction. Knockdown of either protein by small interfering RNA (siRNA) resulted in a decrease in the level of the other, consistent with the idea that they mutually stabilize one another within a complex (Figure 3E).

The interaction of PLEKHA4 with KLHL12 provides a window into the potential roles of PLEKHA4 in the cell. KLHL12 is a member of the family of BTB proteins, which function as adaptors that direct the E3 ubiquitin ligase CUL3 to specific substrates (Furukawa et al., 2003; Xu et al., 2003). To explore whether the PLEKHA4-KLHL12 interaction influences the ability of KLHL12 to regulate CUL3, we ascertained the ability of all three proteins to colocalize. Immunofluorescence analysis of cells co-transfected with tagged PLEKHA4, KLHL12, and CUL3 revealed that PLEKHA4 could recruit the CUL3-KLHL12 complex to the plasma membrane (Figure 3F).

PLEKHA4 Negatively Regulates the E3 Ligase Activity of CUL3-KLHL12

We tested whether PLEKHA4 is simply a ubiquitination substrate of the CUL3-KLHL12 E3 ubiquitin ligase. We found that GFP-PLEKHA4 was minimally, if at all, ubiquitinated, and, more important, that its marginal levels of ubiquitination were not affected by the overexpression of KLHL12 (Figure S3).

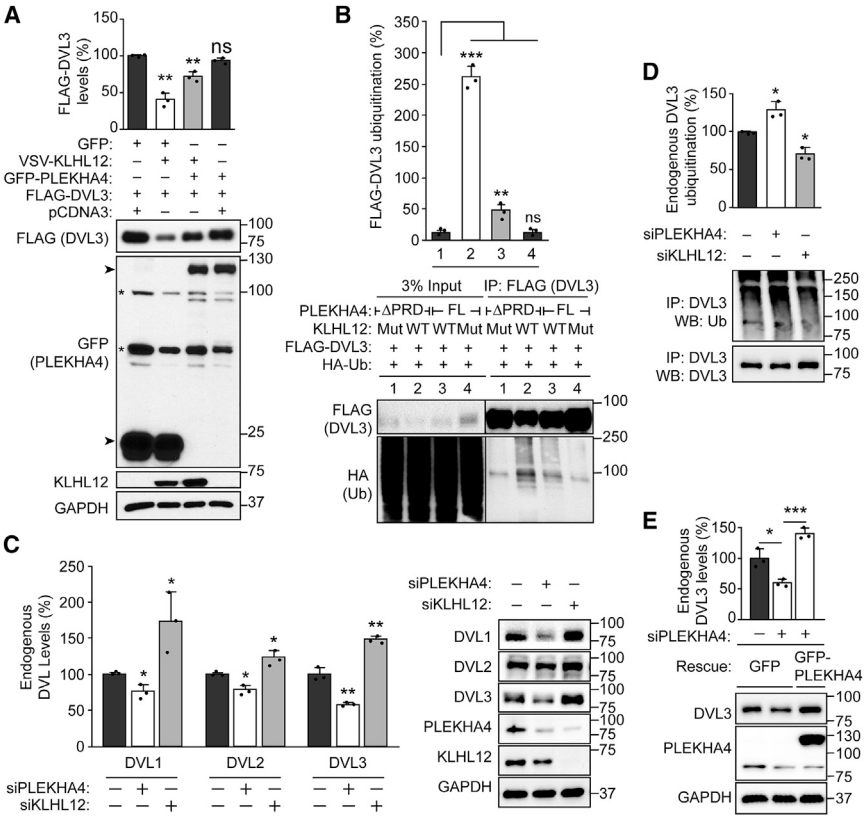

Figure 4. PLEKHA4 Negatively Regulates the CUL3-KLHL12-Mediated Ubiquitination and Degradation of DVL3

Western blot analysis and quantification of HeLa cells transfected with the indicated plasmids and/or siRNA duplexes.

(A) Overexpression of PLEKHA4 attenuates KLHL12-dependent decrease in FLAG-DVL3 levels. On the anti-GFP western blot, arrowheads indicate GFP-PLEKHA4^{FL} (which migrates at ~120 kDa) and GFP (which migrates at ~25 kDa), and asterisks on blots indicate non-specific background immunoreactivity. **p < 0.01, ns, not significant (n = 3).

(B) Overexpression of PLEKHA4^{FL}, which is capable of interaction with KLHL12, but not PLEKHA4$^{\Delta PRD}$, which is not capable, attenuates the ubiquitination of FLAG-DVL3 by a functional VSV-tagged KLHL12 (wild type [WT]) but not an inactive KLHL12 mutant that does not engage CUL3 (Q405X, Mut). One day after transfection with appropriate plasmids, cells were subjected to anti-FLAG immunoprecipitation and western blot analysis. Note the increased levels of DVL3 and decreased ubiquitination of DVL3 in lane 3 compared to lane 2. **p < 0.01, ***p < 0.001, ns, not significant (n = 3).

(C) PLEKHA4 modulates the levels of endogenous DVL1, DVL2, and DVL3. Western blot analysis of lysates from HeLa cells treated with siRNA duplexes against PLEKHA4 (siPLEKHA4), KLHL12 (siKLHL12), or a negative control siRNA (–). *p < 0.05, **p < 0.01 (n = 3).

(D) PLEKHA4 modulates the ubiquitination of endogenous DVL3. Western blot analysis of anti-DVL3 immunoprecipitates from HeLa cells treated with the indicated siRNA duplexes. *p < 0.05 (n = 3).

(E) Full-length GFP-PLEKHA4 can functionally rescue the changes in DVL3 levels induced by siPLEKHA4. Western blot analysis of lysates from HeLa cells subjected to siPLEKHA4 and/or transfection with an siRNA-resistant GFP-PLEKHA4^{FL} construct (which migrates at ~120 kDa). *p < 0.05 (n = 3), ***p < 0.001. All of the quantifications were normalized to the loading control (glyceraldehyde 3-phosphate dehydrogenase [GAPDH]).

See also Figure S3.

If PLEKHA4 is not a ubiquitination substrate of CUL3-KLHL12, then it instead may function as an adaptor to recruit CUL3-KLHL12 to a site of action at the plasma membrane. Among the established ubiquitination substrates of CUL3-KLHL12, the protein Dishevelled-3 (DVL3) can localize to the plasma membrane. We thus interrogated the levels of the total amount of DVL3 and the extent of DVL3 ubiquitination after modulating PLEKHA4 and/or KLHL12 levels.

We co-expressed FLAG-DVL3 with KLHL12, PLEKHA4, or both KLHL12 and PLEKHA4 (Figure 4A). As expected, the overexpression of KLHL12 decreased FLAG-DVL3 levels (Angers et al., 2006). Overexpression of PLEKHA4 along with KLHL12 led to higher levels of FLAG-DVL3 than overexpression of KLHL12 alone, suggesting that PLEKHA4 attenuates the effect of KLHL12 on DVL3 levels. The expression of PLEKHA4 alone had no significant effect relative to control, consistent with the idea that PLEKHA4 acts through CUL3-KLHL12.

Using a similar approach, we investigated how PLEKHA4 influences the ubiquitination of FLAG-DVL3 (Figure 4B). Here, we found that the overexpression of full-length PLEKHA4 along with KLHL12 attenuates the massive increase in FLAG-DVL3 ubiquitination caused by the overexpression of KLHL12 alone. We used as negative controls versions of PLEKHA4 and KLHL12 that are non-functional (i.e., PLEKHA4$^{\Delta PRD}$, which does not interact with KLHL12, and KLHL12^{Q405X}, which does not engage CUL3; Angers et al., 2006). Thus, we conclude that the effect of overexpressed PLEKHA4 on FLAG-DVL3 ubiquitination requires its interaction with an active CUL3-KLHL12 E3 ligase.

Loss-of-function studies using siRNA and examining endogenous DVL proteins led to the same conclusions. Knockdown of PLEKHA4 decreased the levels of all three DVL isoforms (DVL1, DVL2, and DVL3), whereas, as expected (Angers et al., 2006), knockdown of KLHL12 led to increases in the levels of the three DVL proteins (Figure 4C). Furthermore, knockdown of PLEKHA4 led to the increased ubiquitination of endogenous DVL3, whereas knockdown of KLHL12 led to the decreased ubiquitination of DVL3 (Figure 4D). The effect of PLEKHA4 knockdown could be rescued by transfection with an siRNA-resistant GFP-PLEKHA4 construct, confirming the specificity of the PLEKHA4 siRNA and the functionality of the GFP-PLEKHA4 construct (Figure 4E). Collectively, these overexpression and knockdown studies support the hypothesis that PLEKHA4 negatively regulates CUL3-KLHL12-mediated ubiquitination of the DVL proteins.

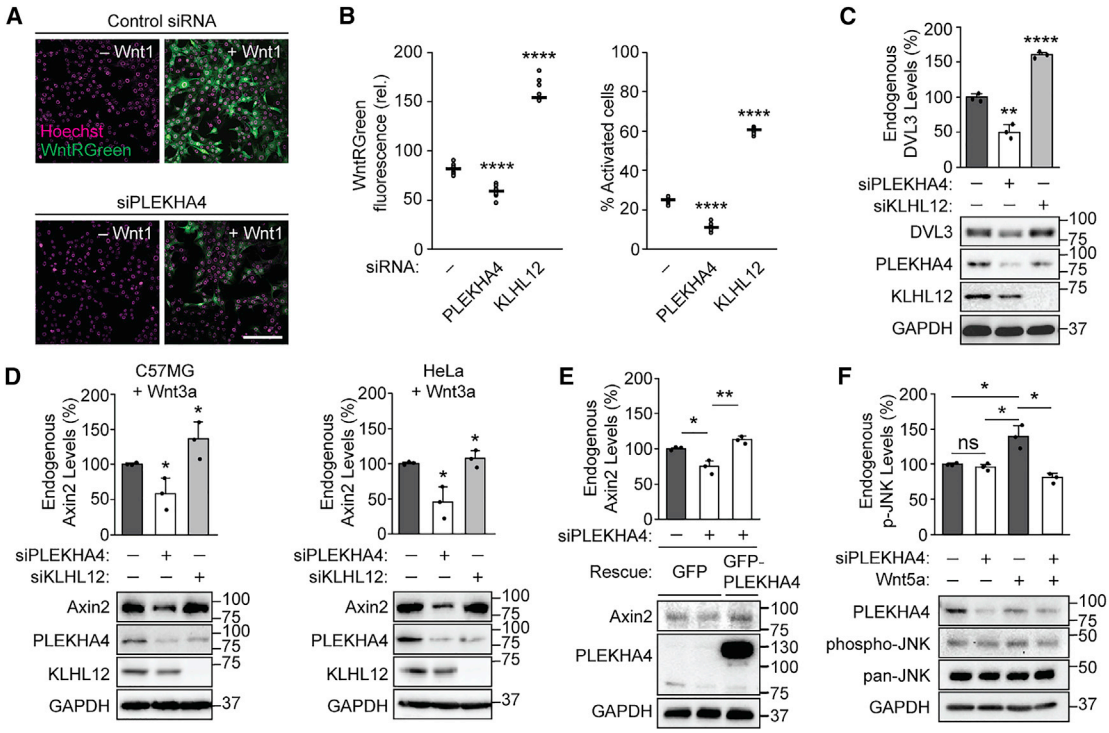

Figure 5. PLEKHA4 Is a Positive Regulator of Canonical and Non-canonical Wnt Signaling in Mammalian Cells

(A) Knockdown of PLEKHA4 decreases Wnt1-induced expression of GFP in C57MG cells stably expressing the WntRGreen reporter. Control siRNA or PLEKHA4 knockdown (siPLEKHA4) was performed in C57MG-WntRGreen cells, which were co-cultured with Wnt1-expressing MV7-Rat2a-Wnt1 cells (+Wnt1) or control MV7-Rat2a cells (–Wnt1), followed by imaging of WntRGreen-derived GFP fluorescence (green) and nuclei (Hoechst 33342, magenta) by confocal microscopy.

(B) Quantification of changes in WntRGreen fluorescence induced by knockdown of PLEKHA4 or KLHL12. Cells were treated with siRNA against PLEKHA4, KLHL12, or negative control siRNA (–), followed by the quantification of GFP fluorescence by flow cytometry. Each dot on the plot represents a separate biological replicate. $^{**}p < 0.01$, $^{***}p < 0.001$, $^{****}p < 0.0001$ (n = 9).

(C) PLEKHA4 and KLHL12 regulate levels of endogenous DVL3 in C57MG-WntRGreen cells. Western blot analysis of cells treated with an siRNA duplex against PLEKHA4 (siPLEKHA4), KLHL12 (siKLHL12), or a negative control siRNA (–). $^{**}p < 0.01$, $^{****}p < 0.0001$ (n = 3).

(D) PLEKHA4 and KLHL12 regulate Wnt3a-stimulated changes in the levels of endogenous Axin2. C57MG or HeLa cells were treated with the indicated siRNA duplex and stimulated with Wnt3a-containing conditioned media. $^{*}p < 0.05$ (n = 3).

(E) Full-length GFP-PLEKHA4 can functionally rescue the attenuation of Wnt3a-stimulated increase in levels of endogenous Axin2 induced by knockdown of PLEKHA4 (siPLEKHA4). Western blot analysis of lysates from HeLa cells subjected to siPLEKHA4 or negative control siRNA (–), stimulation with Wnt3a-containing conditioned media, and transfection with either GFP only or an siRNA-resistant GFP-PLEKHA4^{FL} construct. $^{*}p < 0.05$, $^{**}p < 0.01$ (n = 3).

(F) PLEKHA4 regulates the phosphorylation of JNK, a marker associated with non-canonical Wnt (planar cell polarity) signaling pathway. Western blot analysis of C57MG cells subjected to siPLEKHA4 or negative control siRNA (–) and stimulation with control or Wnt5a-containing conditioned media. $^{*}p < 0.05$, ns, not significant (n = 3).

In graphs showing quantification, all of the levels were normalized to the loading control (GAPDH), except (F), in which levels were normalized to pan-JNK. Scale bar: 200 μm.

PLEKHA4 Is a Positive Regulator of Canonical and Non-canonical Wnt Signaling in Mammalian Cells

DVL3 and its paralogs DVL1 and DVL2 are central intermediates in the canonical and non-canonical branches of Wnt signaling, which collectively can control many developmental processes (Clevers and Nusse, 2012; Mlodzik, 2016). We thus asked whether the modulation of PLEKHA4 levels would affect Wnt signaling strength. For these assays, we used a mouse fibroblast cell line (C57MG) responsive to Wnt stimulation that contained a Wnt-inducible GFP transcriptional reporter called WntRGreen (Brown et al., 1986; Santiago et al., 2012), as well as human cell lines such as HeLa cells.

PLEKHA4 knockdown decreased WntRGreen fluorescence, as visualized by microscopy (Figure 5A) and as quantified by flow cytometry (Figure 5B). As expected, KLHL12 knockdown increased WntRGreen fluorescence, which is consistent with a role for KLHL12 in mediating DVL3 ubiquitination (Figure 5B). We observed similar effects on DVL3 levels in these C57MG cells (Figure 5C) as we had previously seen in HeLa cells (Figure 4C). From these data, we conclude that PLEKHA4 functions in cells as a positive modulator of Wnt signaling via its effects on DVL3 levels.

To complement the β-catenin-dependent reporter, we also examined the effect of PLEKHA4 knockdown on endogenous levels of the Wnt3a target gene Axin2, whose levels are induced by canonical Wnt signaling. We found that knockdown of PLEKHA4 attenuated the Wnt3a-stimulated increase in endogenous Axin2 (Figure 5D) and that this effect could be rescued by transfection with GFP-PLEKHA4 (Figure 5E).

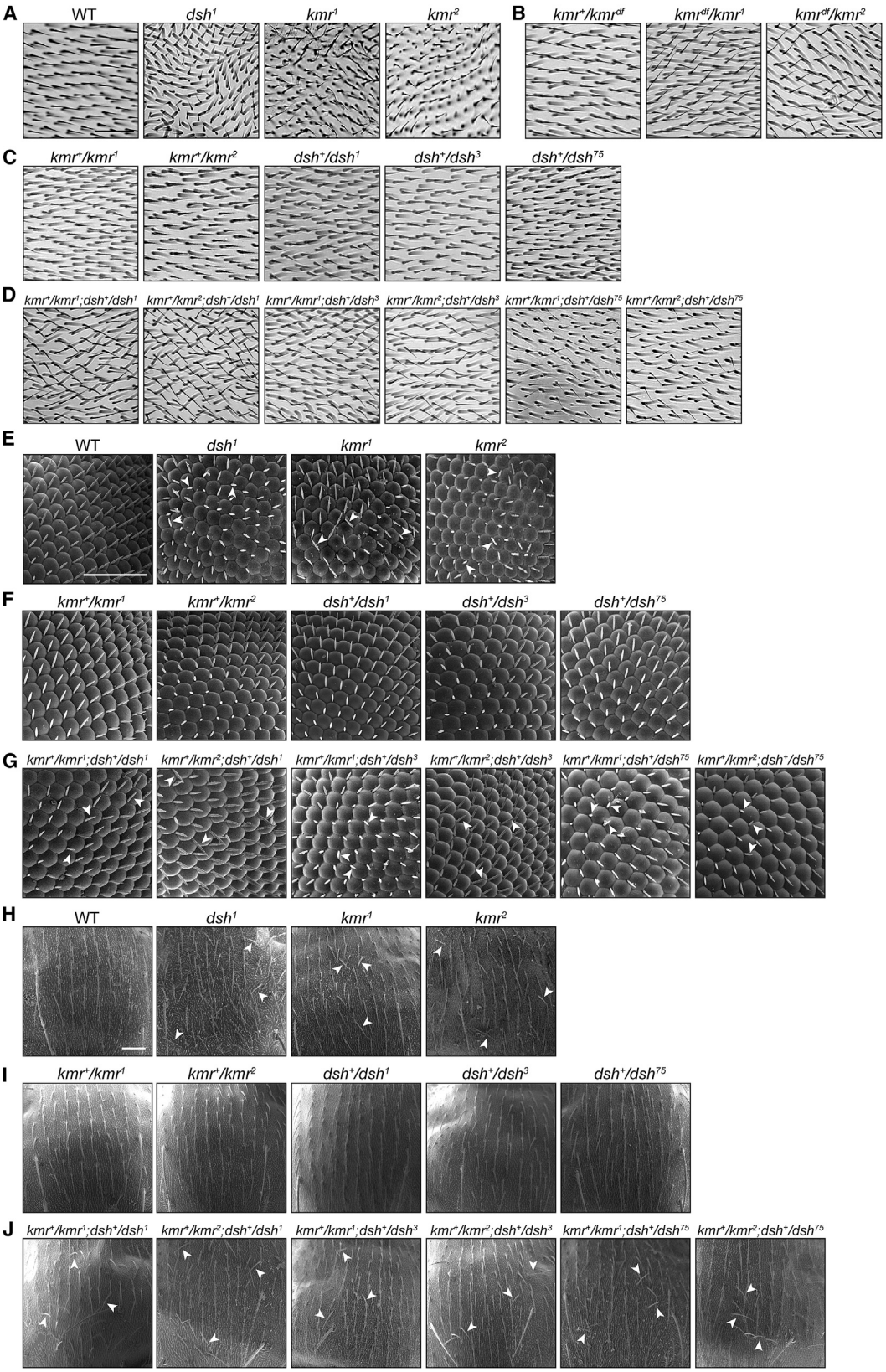

(legend on next page)

Finally, we assessed the effect of PLEKHA4 knockdown on a non-canonical Wnt signaling pathway. We found that knockdown of PLEKHA4 attenuated the Wnt5a-stimulated increase in the phosphorylation of c-Jun N-terminal kinase (JNK), which becomes activated upon the exposure of cells to Wnt5a, a stimulus of β-catenin-independent, non-canonical Wnt signaling (Boutros et al., 1998) (Figure 5F).

These data indicate that, in mammalian cells, PLEKHA4 is a positive regulator of both canonical, β-catenin-dependent, and non-canonical, β-catenin-independent, Wnt signaling.

The Fly PLEKHA4 Homolog, *kramer*, Is a Specific Modulator of PCP Signaling

To establish the physiological relevance of our *in vitro* findings linking PLEKHA4 to Wnt signaling, we investigated the loss of PLEKHA4 function *in vivo* in *Drosophila melanogaster*. Both canonical Wnt (Wingless) signaling and the PCP pathway are well established in this organism (Simons and Mlodzik, 2008; Swarup and Verheyen, 2012; Wodarz and Nusse, 1998). Although PCP signaling is not known to respond to Wnt ligands, it shares key intracellular signaling molecules and outputs with vertebrate non-canonical Wnt signaling and is considered the *Drosophila* counterpart of this pathway (Axelrod, 2009; Hale and Strutt, 2015). To simplify the analysis, the fly genome has only a single PLEKHA4 homolog, *CG34383*, which shares the overall domain architecture and 31% sequence identity with PLEKHA4 (including 53% identity between the PH domains).

We generated two *CG34383* knockout alleles using CRISPR/Cas9-mediated mutagenesis, both carrying frameshift mutations early in the coding sequence and thus predicted to be null (Figure S4). We first assessed the physiological effects of the loss of *CG34383 in vivo* by examining hair patterning in the adult wing. The uniform wing hair orientation (proximal to distal) is controlled by the PCP pathway, which depends on *dishevelled (dsh)*, a core PCP signaling component (Devenport, 2014; Hale and Strutt, 2015). Disruption of PCP signaling leads to misoriented hair patterns—for example, as seen in a strain homozygous for dsh^1 (Figures 6A and S5A), a hypomorphic allele that is defective in PCP (Boutros et al., 1998). We found that knockout of *CG34383* causes aberrant wing hair patterns similar to those in the dsh^1 flies (Figures 6A and S5A). Due to the irregular hair patterning in the *CG34383* mutants, we named this locus *kramer* (*kmr*) and called our two knockout mutant alleles kmr^1 and kmr^2. In all of our experiments, both *kmr* alleles exhibited identical phenotypes and may be referred to interchangeably as kmr^-.

We performed two experiments to demonstrate the specificity of these effects. First, we confirmed that the loss of function in *kmr* was responsible for the wing hair phenotype by generating flies hemizygous for the kmr^- alleles with a deletion covering *kmr* and 22 additional genes (*Df(3R)Exel6170,* called *df*). The kmr^{df}/kmr^1 and kmr^{df}/kmr^2 hemizygotes exhibited wing hair polarity defects identical to those seen in the kmr^1 and kmr^2 strains (Figures 6B and S5B).

Second, we tested the genetic interaction of *kmr* with *dsh* by examining hair patterning in transheterozygotic strains containing one allele each of either kmr^1 or kmr^2 and one of three different *dsh* alleles, the hypomorphic dsh^1 and the amorphic dsh^3 and dsh^{75} alleles. Whereas heterozygotes carrying only one copy of these alleles (kmr^+/kmr^1, kmr^+/kmr^2, dsh^+/dsh^1, dsh^+/dsh^3, and dsh^+/dsh^{75}) exhibited wild-type wing hair patterning (Figures 6C and S5C), transheterozygotes containing one copy each of mutant alleles *kmr* and *dsh* exhibited modest but consistent defects in wing hair patterning (Figures 6D and S5D). This kind of genetic interaction indicates that partial loss of the function of both proteins causes synthetic defects in PCP signaling, strongly suggesting that *kmr* and *dsh* function in the same pathway.

We analyzed defects in hair patterning in two additional adult tissues, the eye and the thorax, using scanning electron microscopy (SEM) imaging. Again, we found that homozygous kmr^1 and kmr^2 flies exhibited a loss of polarized hair patterning in these tissues, similar to the dsh^1 homozygote (Figures 6E, 6H, S6A, and S7A). Transheterozygote analysis revealed synthetic defects between the two *kmr* alleles and the three *dsh* alleles in the PCP phenotypes in these tissues as well (Figures 6F, 6G, 6I, 6J, S6B, S6C, S7B, and S7C).

kramer Modulates PCP Signaling by Affecting Dishevelled Levels and Polarized Localization in the Developing Wing

Finally, to evaluate the mechanism by which *kmr* affects PCP signaling, we examined the levels of the Dsh protein in the

Figure 6. Knockout of the Fly PLEKHA4 Homolog, *kramer*, Results in Defects in Planar Cell Polarity Signaling

(A–D) Bright-field imaging analysis of the *Drosophila melanogaster* adult wing, oriented proximal to distal (left to right), to evaluate the effects of various gene disruptions on PCP signaling.

(A) Two knockout strains of *kramer* (kmr^1 and kmr^2, referred to interchangeably as kmr^-) exhibit aberrant wing bristles similar to a homozygous, hypomorphic mutant of Dishevelled (dsh^1). See Figure S4 for details on the generation of *kmr* KO alleles by CRISPR/Cas9-mediated mutagenesis.

(B) Validation of the specificity of the phenotype in kmr^- via complementation with a chromosomal deletion strain, *Df(3R)Exel6170 (Δ 87F10–87F14)*, denoted here as *df*. Note that kmr^{df}/kmr^-, which bears one CRISPR/Cas9-deleted allele and one chromosomal deletion allele, phenocopies either homozygous kmr^- strain.

(C and D) Genetic interaction between *kmr* and *dsh*. Analysis of five simple heterozygote strains (kmr^+/kmr^1, kmr^+/kmr^2, dsh^+/dsh^1, dsh^+/dsh^3, and dsh^+/dsh^{75}) (C) and six transheterozygote strains ($kmr^+/kmr^-;dsh^+/dsh^1$, $kmr^+/kmr^-;dsh^+/dsh^3$, or $kmr^+/kmr^-;dsh^+/dsh^{75}$ for both the kmr^1 and kmr^2 alleles) (D), demonstrating that the dysfunction of a single allele of both genes within the same organism leads to a modest PCP phenotype (D), compared to simple heterozygotic strains (C), whose patterning resembles wild type.

(E–J) Scanning electron microscopy (SEM) imaging reveals aberrant hair patterning resulting from defects in PCP signaling in the eyes (E–G) and thorax (H–J) of *kmr* mutant and *kmr/dsh* transheterozygote adult flies. For these experiments, the same genotypes as in (A), (C), and (D) were used for analysis, with homozygotes in (E) and (H), simple heterozygotes in (F) and (I), and transheterozygotes in (G) and (J).

The arrowheads indicate examples of hairs with altered orientations due to defective PCP signaling. This figure shows one representative image per genotype, and Figures S5–S7 show three additional images per genotype for wing, eye, and thorax imaging, respectively. Scale bars: 50 μm.

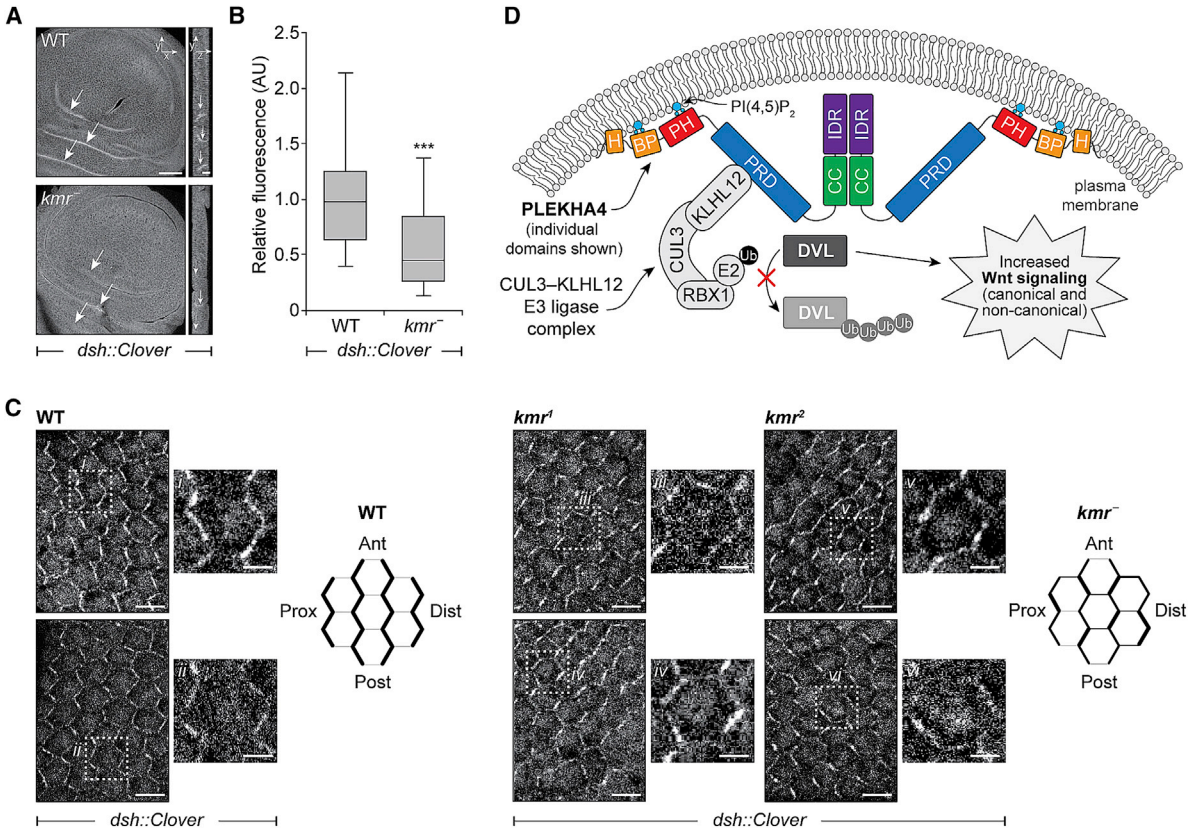

Figure 7. Knockout of *kmr* Causes Defects in Dishevelled Levels and Polarized Localization during *Drosophila* Development

(A and B) Knockout of *kmr* leads to lower levels of Dsh-Clover in wing imaginal discs. Confocal microscopy analysis (A) and quantification (B) of Dsh-Clover fluorescence in L3 larval wing imaginal discs expressing Dsh-Clover (top, wild type [*dsh::Clover*]; bottom, *kmr* knockout [*dsh::Clover;kmr*$^{-}$]). Shown are xy and orthogonal (yz) projections. Arrows indicate the epithelial folds of the wing discs. In the boxplot representing the quantification of the Dsh-Clover fluorescence at epithelial folds, boxes represent the second and third quartiles, with the line in the middle representing the median and the whiskers denoting the maximum and minimum values. ***$p < 0.001$ ($n = 12$).

(C) Knockout of *kmr* leads to a loss of the asymmetric, polarized subcellular localization of Dsh-Clover within the pupal wing epithelium. Confocal microscopy of Dsh-Clover fluorescence of 30 h after puparium formation wings of the same genotypes as in (A). Note that Dsh is asymmetrically enriched at proximal-to-distal boundaries in wild-type background. This asymmetry is partially lost, causing a gain of symmetry in both *kmr*$^{-}$ strains. Two representative images are shown for each genotype, and enlarged images showing a single cell (i–vi) are indicated by the dotted line. The illustrations depict the Dsh subcellular localization pattern in wild-type and the *kmr*$^{-}$ mutant. Ant, anterior; Dist, distal; Post, posterior; Prox, proximal. Scale bars: 50 μm (A, z projection), 10 μm (A, orthogonal projection), 5 μm (C, full-size image), and 2.5 μm (C, enlarged images [i–vi]).

(D) The working model for PLEKHA4/Kmr function. It attenuates DVL ubiquitination by sequestering the CUL3 E3 ubiquitin ligase substrate adaptor KLHL12 in clusters at the plasma membrane to, depending on the context, enhance canonical Wnt signaling and/or non-canonical Wnt/PCP signaling pathways.

homozygous *kmr*^{1} and *kmr*^{2} flies. Due to the unavailability of suitable antibodies for immunofluorescence, we used a strain expressing a functional, fluorescently tagged Dsh under the control of the endogenous *dsh* promoter (*dsh::Clover*) (Axelrod, 2001).

First, we examined Dsh-Clover expression in the wing imaginal disc, a larval tissue that gives rise to the adult wing. Dsh is moderately enriched at the apical membrane of wing disc epithelial cells (Axelrod, 2001; Wu et al., 2004), which are best visualized at the folds because these locations are where apical membranes of opposing epithelial cells meet (Figure 7A, arrows). Compared to the wild type, homozygous *kmr*^{1} and *kmr*^{2} flies exhibited reduced Dsh-Clover levels or enrichment within the epithelial folds (Figure 7B). These data suggest that the loss of *kmr* leads to a downregulation of Dsh levels in this tissue and at this developmental time point.

Second, we evaluated the subcellular localization of Dsh-Clover at 30 h after puparium formation. At this stage, Dsh and other core PCP proteins adopt an asymmetric, polarized localization within the epithelium, in advance of the formation of actin bundles where the trichome (hair) will emerge. In the wild-type background, we observed apparent Dsh-Clover enrichment in the proximal and distal membranes within the hexagonal array of epithelial cells, as expected (Axelrod, 2001; Devenport, 2014; Hale and Strutt, 2015; Strutt et al., 2013) (Figure 7C). Homozygous *kmr*^{1} or *kmr*^{2} flies exhibited a loss of this asymmetry, with Dsh-Clover adopting an apparent stochastic, or less polarized, distribution within the plasma membrane. These results indicate that *kmr* modulates PCP signaling via effects on Dsh levels and polarized localization, which speaks to the physiological relevance of our findings.

DISCUSSION

Phosphoinositides are present in low abundance but act as important constituents of eukaryotic membranes (Balla, 2013; Dickson and Hille, 2019; Schink et al., 2016). A major function of these lipids is to act as membrane identity markers by presenting their head groups as ligands to facilitate the recruitment of cytosolic proteins to the correct target membrane. The most prevalent PIP-binding module is the PH domain, which is the 11th most abundant domain in the human proteome, and the physiological functions of the vast majority of PH domain-containing proteins remain unknown (Lemmon, 2008). Our studies reveal a link between PIPs and the control of ubiquitination and Wnt signaling pathways that is mediated by the PH domain-containing protein PLEKHA4.

We found that PLEKHA4 interacts specifically with $PI(4,5)P_2$ at the plasma membrane within cells. Three motifs at the N terminus of PLEKHA4—an amphipathic helix, a basic peptide, and the PH domain—collectively confer the specificity of this recognition. The full-length PLEKHA4 protein assembles into higher-order structures at the plasma membrane that are visible by confocal microscopy as puncta. This assembly is mediated by two C-terminal domains of PLEKHA4: a coiled-coil region and an IDR. These C-terminal domains can self-associate in cells, as ascertained by colocalization, co-IP, and optoDroplet assays (Park et al., 2017; Shin et al., 2017). While the nature of the PLEKHA4 clusters remains unknown, the puncta fail to colocalize with markers of known plasma membrane assemblies, organelles, or membrane contact sites, and it is interesting to speculate they may represent liquid-liquid phase-separated domains (i.e., membraneless organelles) containing PLEKHA4 and other interaction partners (Banjade and Rosen, 2014; Hyman et al., 2014; Li et al., 2012; Mitrea and Kriwacki, 2016; Shin and Brangwynne, 2017).

We characterized a protein-protein interaction between PLEKHA4 and the CUL3 E3 ubiquitin ligase adaptor KLHL12, to which PLEKHA4 binds via its central, proline-rich domain. Mechanistic studies in mammalian cells using both overexpression and RNAi-mediated knockdown of PLEKHA4 indicate a role for this protein as a positive regulator of DVL levels by preventing its polyubiquitination by the CUL3-KLHL12 E3 ligase. These *in vitro* studies also indicated that PLEKHA4 is a positive modulator of both canonical, β-catenin-dependent and non-canonical, β-catenin-independent Wnt signaling pathways. These *in vitro* studies support a model wherein PLEKHA4 recruits the CUL3-KLHL12 E3 ligase complex to the plasma membrane and downregulates its ubiquitination of the DVL proteins, permitting DVL levels to rise and increasing the strength of DVL-dependent canonical and non-canonical Wnt signaling pathways (Figure 7D).

A fascinating aspect of this model is that PLEKHA4 can bring CUL3-KLHL12 to the very membrane where its substrates, the DVL proteins, are activated in Wnt signaling, and yet this recruitment results in less DVL polyubiquitination. We propose that PLEKHA4 sequesters KLHL12 in plasma membrane-associated clusters, in effect creating an ''exclusion zone'' devoid of CUL3-KLHL12 E3 ligase activity and preventing the polyubiquitination of DVL pools at or near this membrane. DVL proteins form cytoplasmic phase-separated clusters (Sear, 2007), and it is possible that sequestration of KLHL12 at the plasma membrane by PLEKHA4 serves to spatially segregate the E3 ligase from these cytoplasmic clusters.

The knockout studies of the PLEKHA4 homolog in *Drosophila melanogaster*, *kramer (kmr)*, provided both a validation of our *in vitro* model in a physiologically relevant setting and revealed layers of regulation of Dishevelled-dependent signaling in this organism. We found that knockout of *kmr* led to selective defects in PCP signaling, which corresponds to non-canonical Wnt signaling in *Drosophila* (Axelrod, 2009; Hale and Strutt, 2015; Simons and Mlodzik, 2008). *Kmr* knockout flies exhibited defects in hair patterning in the adult wing, eye, and thorax. Mechanistically, we established that *kmr* and *dsh* act in the same genetic pathway, as we observed synthetic defects in PCP signaling in transheterozygotic strains. Finally, we assessed the effect of *kmr* knockout on Dsh levels and localization in the developing wing. We found lower levels of Dsh enriched at the apical epithelium in the larval wing imaginal disc and a loss of asymmetric, polarized Dsh distribution at the plasma membrane in the pupal wing epithelium.

In contrast to these PCP phenotypes, we did not observe any phenotypes associated with Wingless signaling, which corresponds to the canonical, β-catenin-dependent pathway in flies, in kmr^1 and kmr^2 flies (Swarup and Verheyen, 2012). Given the substantial remaining levels of Dsh in the kmr^- larval wing imaginal disc and pupal wing, it is possible that the partial, modulatory effect of *kmr* knockout on Dsh levels and localization is not sufficient to cause defects in Wingless signaling in *Drosophila*. In addition, *kmr* specifically regulates the localization of Dsh and thus affects PCP signaling in flies. Nonetheless, our results in cultured mammalian cell lines demonstrating the effect of PLEKHA4 knockdown on both the β-catenin-dependent and -independent signaling pathways suggest that the regulatory role of PLEKHA4 *in vivo* may go beyond the non-canonical Wnt signaling pathway in other organisms.

A detailed study of the *Drosophila* homologs of KLHL12 (*diablo* and *kelch*) established roles for the CUL3-Diablo (or Kelch) E3 ligase complex in modulating PCP signaling *in vivo* in this organism (Strutt et al., 2013). Notably, the study found that subtle changes to the levels of core PCP proteins such as Dsh led to a breakdown of their asymmetric localization in the pupal wing, leading to PCP phenotypes. They also found that Cul3-Diablo/Kelch-mediated modulation of Dsh levels in *Drosophila* led to selective effects on PCP signaling, with no observed effects on Wingless signaling. By contrast, Moon and colleagues found that in vertebrate systems (mammalian cells and zebrafish embryos), the homologous CUL3-KLHL12 E3 ligase complex modulated DVL levels and the strength of canonical, β-catenin-dependent Wnt signaling (Angers et al., 2006).

Our data suggest that PLEKHA4/*kmr* acts as a tuner to attenuate the CUL3-KLHL12-mediated polyubiquitination of DVL proteins by sequestration of KLHL12. We propose that, by creating different DVL setpoints, PLEKHA4/*kmr* can modulate the sensitivity of cells to stimulation by appropriate ligands that propagate canonical Wnt and/or non-canonical Wnt, or PCP, signaling pathways. In this model, the pathway most affected by PLEKHA4/*kmr* is determined by the relative dependence of

that pathway on changes in DVL levels in that tissue context. Furthermore, PLEKHA4/*kmr* may affect DVL levels to different extents in different contexts. Given the critical importance of Wnt signaling pathways in mammalian development and disease, PLEKHA4 may function as a regulator of these pathways *in vivo* in mammals as well.

Finally, the production and maintenance of $PI(4,5)P_2$ at the plasma membrane is important for both canonical and non-canonical Wnt signaling pathways. $PI(4,5)P_2$ enhances the strength of canonical Wnt signaling via effects on the Wnt co-receptor LRP6, and Wnt3a stimulation increases $PI(4,5)P_2$ synthesis via the direct action of DVL on lipid kinases that synthesize $PI(4,5)P_2$, effectively amplifying this lipid-based signal (Pan et al., 2008; Qin et al., 2009). $PI(4,5)P_2$ is also a key determinant of cell polarity, aiding in both establishing the asymmetric spatial arrangement of polarity proteins and in activating actin-nucleating factors (Gassama-Diagne and Payrastre, 2009; Hassan et al., 1998; Shewan et al., 2011; Yin and Janmey, 2003). Given the central role of DVL in PCP signaling (Gao and Chen, 2010; Mlodzik, 2016), its ability to stimulate $PI(4,5)P_2$ synthesis (Hu et al., 2015; Qin et al., 2009), and the critical role of actin dynamics in PCP signaling (Simons and Mlodzik, 2008; Yang and Mlodzik, 2015), changes to $PI(4,5)P_2$ synthesis may directly affect this pathway as well. As a factor that binds to plasma membrane $PI(4,5)P_2$ and affects DVL levels, PLEKHA4 adds a further layer of regulation to DVL-dependent pathways, including Wnt and PCP signaling.

STAR★METHODS

Detailed methods are provided in the online version of this paper and include the following:

- KEY RESOURCES TABLE
- CONTACT FOR REAGENT AND RESOURCE SHARING
- EXPERIMENTAL MODEL AND SUBJECT DETAILS
  - Cell culture
  - *Drosophila melanogaster* husbandry
- METHOD DETAILS
  - Plasmids and cloning
  - Transfection of plasmids and siRNAs
  - Confocal microscopy
  - Immunoprecipitation and western blots
  - SILAC labeling and mass spectrometry-based proteomics analysis
  - Protein expression and purification in *E. coli*
  - Liposome co-sedimentation assays
  - $PI(4,5)P_2$ depletion assay
  - Western blot analysis of DVL levels
  - Analysis of DVL3 ubiquitination
  - Rescue of DVL3 levels by PLEKHA4 transfection
  - Western blot analysis of β-catenin dependent Axin2 levels
  - Rescue of Axin2 levels by PLEKHA4 transfection
  - Western blot analysis of β-catenin independent p-JNK levels
  - Fluorescent Wnt reporter assay
  - Generation of kramer (kmr) knockout flies
  - Generation of flies containing kmr^{-} and other alleles
  - Dissection and imaging of wing imaginal discs, pupal wings, and adult wings
  - Scanning electron microscopy (SEM)
- QUANTIFICATION AND STATISTICAL ANALYSIS
  - Statistics and reproducibility
- DATA AND SOFTWARE AVAILABILITY
  - Data availability statement

SUPPLEMENTAL INFORMATION

Supplemental Information can be found online at https://doi.org/10.1016/j.celrep.2019.04.060.

ACKNOWLEDGMENTS

This work was supported in part by the NIH (R00GM110121 and R01GM131101 to J.M.B., R01NS099125 and R21OD023824 to C.H., R01GM048430 to M.L.G., and R01GM097272 and R01GM123018 to M.B.S.) and awards to J.M.B. from the Arnold and Mabel Beckman Foundation (Beckman Young Investigator) and the Alfred P. Sloan Foundation (Sloan Research Fellowship). Superresolution structured illumination microscopy (SR-SIM) imaging was performed at the Cornell University Biotechnology Resource Center, with support from the National Science Foundation (NSF) (DBI-1428922). SEM imaging was performed at the Cornell Center for Materials Research Facilities, with support from the NSF (DMR-1719875). We thank Jeffrey Axelrod and Song Song (Stanford University) for generously providing *dsh::clover* fly stocks and for helpful discussions; Anthony Brown (Weill Cornell Medicine) for generously providing C57MG-WntRGreen cells and for helpful discussions; the Barbash, Emr, Fromme, Lammerding, and Mao labs for sharing equipment and reagents; and Scott Emr, Chris Fromme, Shaogeng Tang, and Laura Thomas for helpful discussions and/or critical reading of the manuscript.

AUTHOR CONTRIBUTIONS

Conceptualization, A.S. and J.M.B.; Investigation, A.S., A.G.B., D.K., A.P., and W.C.; Writing – Original Draft, A.S. and J.M.B.; Supervision, C.H., M.L.G., M.B.S., and J.M.B.; Funding Acquisition, C.H., M.L.G., M.B.S., and J.M.B.

DECLARATION OF INTERESTS

The authors declare no competing interests.

Received: July 25, 2018
Revised: February 26, 2019
Accepted: April 11, 2019
Published: May 14, 2019

REFERENCES

Angers, S., Thorpe, C.J., Biechele, T.L., Goldenberg, S.J., Zheng, N., MacCoss, M.J., and Moon, R.T. (2006). The KLHL12-Cullin-3 ubiquitin ligase negatively regulates the Wnt-β-catenin pathway by targeting Dishevelled for degradation. Nat. Cell Biol. *8*, 348–357.

Axelrod, J.D. (2001). Unipolar membrane association of Dishevelled mediates Frizzled planar cell polarity signaling. Genes Dev. *15*, 1182–1187.

Axelrod, J.D. (2009). Progress and challenges in understanding planar cell polarity signaling. Semin. Cell Dev. Biol. *20*, 964–971.

Balla, T. (2013). Phosphoinositides: tiny lipids with giant impact on cell regulation. Physiol. Rev. *93*, 1019–1137.

Banjade, S., and Rosen, M.K. (2014). Phase transitions of multivalent proteins can promote clustering of membrane receptors. eLife *3*, e04123.

Bastos de Oliveira, F.M., Kim, D., Cussiol, J.R., Das, J., Jeong, M.C., Doerfler, L., Schmidt, K.H., Yu, H., and Smolka, M.B. (2015). Phosphoproteomics

reveals distinct modes of Mec1/ATR signaling during DNA replication. Mol. Cell *57*, 1124–1132.

Bastos de Oliveira, F.M., Kim, D., Lanz, M., and Smolka, M.B. (2018). Quantitative Analysis of DNA Damage Signaling Responses to Chemical and Genetic Perturbations. Methods Mol. Biol. *1672*, 645–660.

Bolatto, C., Parada, C., and Colmenares, V. (2017). A Rapid and Efficient Method to Dissect Pupal Wings of Drosophila Suitable for Immunodetections or PCR Assays. J. Vis. Exp. Published online December 30, 2017. https://doi.org/10.3791/55854.

Boutros, M., Paricio, N., Strutt, D.I., and Mlodzik, M. (1998). Dishevelled activates JNK and discriminates between JNK pathways in planar polarity and wingless signaling. Cell *94*, 109–118.

Brown, A.M.C., Wildin, R.S., Prendergast, T.J., and Varmus, H.E. (1986). A retrovirus vector expressing the putative mammary oncogene int-1 causes partial transformation of a mammary epithelial cell line. Cell *46*, 1001–1009.

Cadigan, K.M., and Peifer, M. (2009). Wnt signaling from development to disease: insights from model systems. Cold Spring Harb. Perspect. Biol. *1*, a002881.

Clevers, H., and Nusse, R. (2012). Wnt/β-catenin signaling and disease. Cell *149*, 1192–1205.

D'Angelo, G., Polishchuk, E., Di Tullio, G., Santoro, M., Di Campli, A., Godi, A., West, G., Bielawski, J., Chuang, C.C., van der Spoel, A.C., et al. (2007). Glycosphingolipid synthesis requires FAPP2 transfer of glucosylceramide. Nature *449*, 62–67.

Devenport, D. (2014). The cell biology of planar cell polarity. J. Cell Biol. *207*, 171–179.

Dickson, E.J., and Hille, B. (2019). Understanding phosphoinositides : rare, dynamic, and essential membrane phospholipids. Biochem. J. *476*, 1–23.

Dowler, S., Currie, R.A., Campbell, D.G., Deak, M., Kular, G., Downes, C.P., and Alessi, D.R. (2000). Identification of pleckstrin-homology-domain-containing proteins with novel phosphoinositide-binding specificities. Biochem. J. *351*, 19–31.

Dubiel, W., Dubiel, D., Wolf, D.A., and Naumann, M. (2018). Cullin 3-Based Ubiquitin Ligases as Master Regulators of Mammalian Cell Differentiation. Trends Biochem. Sci. *43*, 95–107.

Elbaum-Garfinkle, S., Kim, Y., Szczepaniak, K., Chen, C.C.-H., Eckmann, C.R., Myong, S., and Brangwynne, C.P. (2015). The disordered P granule protein LAF-1 drives phase separation into droplets with tunable viscosity and dynamics. Proc. Natl. Acad. Sci. USA *112*, 7189–7194.

Falkenburger, B.H., Jensen, J.B., and Hille, B. (2010a). Kinetics of M1 muscarinic receptor and G protein signaling to phospholipase C in living cells. J. Gen. Physiol. *135*, 81–97.

Falkenburger, B.H., Jensen, J.B., and Hille, B. (2010b). Kinetics of PIP2 metabolism and KCNQ2/3 channel regulation studied with a voltage-sensitive phosphatase in living cells. J. Gen. Physiol. *135*, 99–114.

Furukawa, M., He, Y.J., Borchers, C., and Xiong, Y. (2003). Targeting of protein ubiquitination by BTB-Cullin 3-Roc1 ubiquitin ligases. Nat. Cell Biol. *5*, 1001–1007.

Ganner, A., Lienkamp, S., Schäfer, T., Romaker, D., Wegierski, T., Park, T.J., Spreitzer, S., Simons, M., Gloy, J., Kim, E., et al. (2009). Regulation of ciliary polarity by the APC/C. Proc. Natl. Acad. Sci. USA *106*, 17799–17804.

Gao, C., and Chen, Y.G. (2010). Dishevelled: the hub of Wnt signaling. Cell. Signal. *22*, 717–727.

Gao, C., Cao, W., Bao, L., Zuo, W., Xie, G., Cai, T., Fu, W., Zhang, J., Wu, W., Zhang, X., and Chen, Y.G. (2010). Autophagy negatively regulates Wnt signalling by promoting Dishevelled degradation. Nat. Cell Biol. *12*, 781–790.

Gassama-Diagne, A., and Payrastre, B. (2009). Phosphoinositide Signaling Pathways. Promising Role as Builders of Epithelial Cell Polarity. Int. Rev. Cell. Mol. Biol. *273*, 313–343.

Godi, A., Di Campli, A., Konstantakopoulos, A., Di Tullio, G., Alessi, D.R., Kular, G.S., Daniele, T., Marra, P., Lucocq, J.M., and De Matteis, M.A. (2004). FAPPs control Golgi-to-cell-surface membrane traffic by binding to ARF and PtdIns(4)P. Nat. Cell Biol. *6*, 393–404.

Gómez-Orte, E., Sáenz-Narciso, B., Moreno, S., and Cabello, J. (2013). Multiple functions of the noncanonical Wnt pathway. Trends Genet. *29*, 545–553.

Hale, R., and Strutt, D. (2015). Conservation of Planar Polarity Pathway Function Across the Animal Kingdom. Annu. Rev. Genet. *49*, 529–551.

Hammond, G.R.V., and Balla, T. (2015). Polyphosphoinositide binding domains: key to inositol lipid biology. Biochim. Biophys. Acta *1851*, 746–758.

Hammond, G.R.V., Fischer, M.J., Anderson, K.E., Holdich, J., Koteci, A., Balla, T., and Irvine, R.F. (2012). PI4P and PI(4,5)P2 are essential but independent lipid determinants of membrane identity. Science *337*, 727–730.

Hassan, B.A., Prokopenko, S.N., Breuer, S., Zhang, B., Paululat, A., and Bellen, H.J. (1998). skittles, a Drosophila phosphatidylinositol 4-phosphate 5-kinase, is required for cell viability, germline development and bristle morphology, but not for neurotransmitter release. Genetics *150*, 1527–1537.

Hoedt, E., Zhang, G., and Neubert, T.A. (2014). Stable Isotope Labeling by Amino Acids in Cell Culture (SILAC) for Quantitative Proteomics. In Advancements of Mass Spectrometry in Biomedical Research, A.G. Woods and C.C. Darie, eds. (Springer), pp. 93–106.

Hu, J., Yuan, Q., Kang, X., Qin, Y., Li, L., Ha, Y., and Wu, D. (2015). Resolution of structure of PIP5K1A reveals molecular mechanism for its regulation by dimerization and dishevelled. Nat. Commun. *6*, 8205.

Hyman, A.A., Weber, C.A., and Jülicher, F. (2014). Liquid-liquid phase separation in biology. Annu. Rev. Cell Dev. Biol. *30*, 39–58.

Idevall-Hagren, O., Dickson, E.J., Hille, B., Toomre, D.K., and De Camilli, P. (2012). Optogenetic control of phosphoinositide metabolism. Proc. Natl. Acad. Sci. USA *109*, E2316–E2323.

Janda, C.Y., Waghray, D., Levin, A.M., Thomas, C., and Garcia, K.C. (2012). Structural basis of Wnt recognition by Frizzled. Science *337*, 59–64.

Jin, L., Pahuja, K.B., Wickliffe, K.E., Gorur, A., Baumgärtel, C., Schekman, R., and Rape, M. (2012). Ubiquitin-dependent regulation of COPII coat size and function. Nature *482*, 495–500.

Jungmichel, S., Sylvestersen, K.B., Choudhary, C., Nguyen, S., Mann, M., and Nielsen, M.L. (2014). Specificity and commonality of the phosphoinositide-binding proteome analyzed by quantitative mass spectrometry. Cell Rep. *6*, 578–591.

Lemmon, M.A. (2007). Pleckstrin homology (PH) domains and phosphoinositides. Biochem. Soc. Symp. *74*, 81–93.

Lemmon, M.A. (2008). Membrane recognition by phospholipid-binding domains. Nat. Rev. Mol. Cell Biol. *9*, 99–111.

Li, H., and Marshall, A.J. (2015). Phosphatidylinositol (3,4) bisphosphate-specific phosphatases and effector proteins: a distinct branch of PI3K signaling. Cell. Signal. *27*, 1789–1798.

Li, P., Banjade, S., Cheng, H.C., Kim, S., Chen, B., Guo, L., Llaguno, M., Hollingsworth, J.V., King, D.S., Banani, S.F., et al. (2012). Phase transitions in the assembly of multivalent signalling proteins. Nature *483*, 336–340.

Lin, Y., Protter, D.S.W., Rosen, M.K., and Parker, R. (2015). Formation and Maturation of Phase-Separated Liquid Droplets by RNA-Binding Proteins. Mol. Cell *60*, 208–219.

MacDonald, B.T., Tamai, K., and He, X. (2009). Wnt/β-catenin signaling: components, mechanisms, and diseases. Dev. Cell *17*, 9–26.

Mai, A., Jung, S.K., and Yonehara, S. (2004). hDKIR, a human homologue of the Drosophila kelch protein, involved in a ring-like structure. Exp. Cell Res. *300*, 72–83.

McGourty, C.A., Akopian, D., Walsh, C., Gorur, A., Werner, A., Schekman, R., Bautista, D., and Rape, M. (2016). Regulation of the CUL3 Ubiquitin Ligase by a Calcium-Dependent Co-adaptor. Cell *167*, 525–538.e14.

Milburn, C.C., Komander, D., Deak, M., Alessi, D.R., and Van Aalten, D.M.F. (2004). 1UPR: Crystal structure of the PEPP1 pleckstrin homology domain in complex with inositol 1,3,4,5-tetrakisphosphate. https://www.ncbi.nlm.nih.gov/Structure/pdb/1UPR.

Mitrea, D.M., and Kriwacki, R.W. (2016). Phase separation in biology; functional organization of a higher order. Cell Commun. Signal. *14*, 1.

Miyazaki, K., Fujita, T., Ozaki, T., Kato, C., Kurose, Y., Sakamoto, M., Kato, S., Goto, T., Itoyama, Y., Aoki, M., and Nakagawara, A. (2004). NEDL1, a novel ubiquitin-protein isopeptide ligase for dishevelled-1, targets mutant superoxide dismutase-1. J. Biol. Chem. *279*, 11327–11335.

Mlodzik, M. (2016). The Dishevelled Protein Family: Still Rather a Mystery After Over 20 Years of Molecular Studies. Curr. Top. Dev. Biol. *117*, 75–91.

Nott, T.J., Petsalaki, E., Farber, P., Jervis, D., Fussner, E., Plochowietz, A., Craggs, T.D., Bazett-Jones, D.P., Pawson, T., Forman-Kay, J.D., and Baldwin, A.J. (2015). Phase transition of a disordered nuage protein generates environmentally responsive membraneless organelles. Mol. Cell *57*, 936–947.

Pan, W., Choi, S.C., Wang, H., Qin, Y., Volpicelli-Daley, L., Swan, L., Lucast, L., Khoo, C., Zhang, X., Li, L., et al. (2008). Wnt3a-mediated formation of phosphatidylinositol 4,5-bisphosphate regulates LRP6 phosphorylation. Science *321*, 1350–1353.

Park, H., Kim, N.Y., Lee, S., Kim, N., Kim, J., and Heo, W.D. (2017). Optogenetic protein clustering through fluorescent protein tagging and extension of CRY2. Nat. Commun. *8*, 30.

Qin, Y., Li, L., Pan, W., and Wu, D. (2009). Regulation of phosphatidylinositol kinases and metabolism by Wnt3a and Dvl. J. Biol. Chem. *284*, 22544–22548.

Rondou, P., Haegeman, G., Vanhoenacker, P., and Van Craenenbroeck, K. (2008). BTB Protein KLHL12 targets the dopamine D4 receptor for ubiquitination by a Cul3-based E3 ligase. J. Biol. Chem. *283*, 11083–11096.

Santiago, F., Oguma, J., Brown, A.M.C., and Laurence, J. (2012). Noncanonical Wnt signaling promotes osteoclast differentiation and is facilitated by the human immunodeficiency virus protease inhibitor ritonavir. Biochem. Biophys. Res. Commun. *417*, 223–230.

Schindelin, J., Arganda-Carreras, I., Frise, E., Kaynig, V., Longair, M., Pietzsch, T., Preibisch, S., Rueden, C., Saalfeld, S., Schmid, B., et al. (2012). Fiji: an open-source platform for biological-image analysis. Nat. Methods *9*, 676–682.

Schink, K.O., Raiborg, C., and Stenmark, H. (2013). Phosphatidylinositol 3-phosphate, a lipid that regulates membrane dynamics, protein sorting and cell signalling. BioEssays *35*, 900–912.

Schink, K.O., Tan, K.-W., and Stenmark, H. (2016). Phosphoinositides in Control of Membrane Dynamics. Annu. Rev. Cell Dev. Biol. *32*, 143–171.

Sear, R.P. (2007). Dishevelled: a protein that functions in living cells by phase separating. Soft Matter *3*, 680–684.

Shah, J., Guerrera, D., Vasileva, E., Sluysmans, S., Bertels, E., and Citi, S. (2016). PLEKHA7: cytoskeletal adaptor protein at center stage in junctional organization and signaling. Int. J. Biochem. Cell Biol. *75*, 112–116.

Sharma, J., Mulherkar, S., Mukherjee, D., and Jana, N.R. (2012). Malin regulates Wnt signaling pathway through degradation of dishevelled2. J. Biol. Chem. *287*, 6830–6839.

Shewan, A., Eastburn, D.J., and Mostov, K. (2011). Phosphoinositides in cell architecture. Cold Spring Harb. Perspect. Biol. *3*, a004796.

Shin, Y., and Brangwynne, C.P. (2017). Liquid phase condensation in cell physiology and disease. Science *357*, eaaf4382.

Shin, Y., Berry, J., Pannucci, N., Haataja, M.P., Toettcher, J.E., and Brangwynne, C.P. (2017). Spatiotemporal Control of Intracellular Phase Transitions Using Light-Activated optoDroplets. Cell *168*, 159–171.e14.

Simons, M., and Mlodzik, M. (2008). Planar cell polarity signaling: from fly development to human disease. Annu. Rev. Genet. *42*, 517–540.

Spratford, C.M., and Kumar, J.P. (2014). Dissection and immunostaining of imaginal discs from Drosophila melanogaster. J. Vis. Exp. *91*, 51792.

Strutt, H., Searle, E., Thomas-Macarthur, V., Brookfield, R., and Strutt, D. (2013). A Cul-3-BTB ubiquitylation pathway regulates junctional levels and asymmetry of core planar polarity proteins. Development *140*, 1693–1702.

Swarup, S., and Verheyen, E.M. (2012). Wnt/Wingless signaling in Drosophila. Cold Spring Harb. Perspect. Biol. *4*, a007930.

Wallingford, J.B. (2012). Planar cell polarity and the developmental control of cell behavior in vertebrate embryos. Annu. Rev. Cell Dev. Biol. *28*, 627–653.

Wallingford, J.B., and Habas, R. (2005). The developmental biology of Dishevelled: an enigmatic protein governing cell fate and cell polarity. Development *132*, 4421–4436.

Wei, W., Li, M., Wang, J., Nie, F., and Li, L. (2012). The E3 ubiquitin ligase ITCH negatively regulates canonical Wnt signaling by targeting dishevelled protein. Mol. Cell. Biol. *32*, 3903–3912.

Wodarz, A., and Nusse, R. (1998). Mechanisms of Wnt signaling in development. Annu. Rev. Cell Dev. Biol. *14*, 59–88.

Wu, J., Klein, T.J., and Mlodzik, M. (2004). Subcellular localization of frizzled receptors, mediated by their cytoplasmic tails, regulates signaling pathway specificity. PLoS Biol. *2*, E158.

Xu, L., Wei, Y., Reboul, J., Vaglio, P., Shin, T.H., Vidal, M., Elledge, S.J., and Harper, J.W. (2003). BTB proteins are substrate-specific adaptors in an SCF-like modular ubiquitin ligase containing CUL-3. Nature *425*, 316–321.

Yang, Y., and Mlodzik, M. (2015). Wnt-Frizzled/planar cell polarity signaling: cellular orientation by facing the wind (Wnt). Annu. Rev. Cell Dev. Biol. *31*, 623–646.

Yin, H.L., and Janmey, P.A. (2003). Phosphoinositide regulation of the actin cytoskeleton. Annu. Rev. Physiol. *65*, 761–789.

Zhao, H., and Lappalainen, P. (2012). A simple guide to biochemical approaches for analyzing protein-lipid interactions. Mol. Biol. Cell *23*, 2823–2830.

STAR★METHODS

KEY RESOURCES TABLE

REAGENT or RESOURCE	SOURCE	IDENTIFIER
Antibodies		
Rabbit polyclonal anti-PLEKHA4	Abcam	Cat#ab170537
Mouse monoclonal anti-KLHL12	ProMab Biotechnology	Cat#30058
Mouse monoclonal anti-DVL1	Santa Cruz Biotechnology	Cat#sc-8025 [3F12]
Rabbit polyclonal anti-DVL2	Cell Signaling Technology	Cat#3216
Mouse monoclonal anti-DVL3	Santa Cruz Biotechnology	Cat#sc-8027 [4D3]
Rabbit monoclonal anti-Axin2	Cell Signaling Technology	Cat#2151 [76G6]
Rabbit monoclonal anti-Axin2	Abcam	Cat#ab109307
Mouse monoclonal anti-p-JNK	Santa Cruz Biotechnology	Cat#sc-6254 [G7]
Mouse monoclonal anti-pan-JNK	Santa Cruz Biotechnology	Cat#sc-7345 [D2]
Mouse monoclonal anti-GFP	Takara Bio	Cat #632375 Living Colors
Mouse monoclonal anti-mCherry	Abcam	Cat#ab125096 [1C51]
Rabbit polyclonal anti-FLAG	Millipore Sigma	Cat#F7425
Rat monoclonal anti-HA	Roche	Cat#11867423001 [3F10]
Mouse monoclonal anti-Ubiquitin	Santa Cruz Biotechnology	Cat#sc-8017 [P4D1]
Mouse monoclonal anti-GAPDH	GeneTex	Cat#GTX78213 [1D4]
Rabbit polyclonal anti-Caveolin 1	BD Biosciences	Cat#610059
Rabbit polyclonal anti-EEA1	Thermo Fisher Scientific	PA1-063A
Mouse monoclonal anti-Rab3	Pietro De Camilli, Yale	CL42.1 ascites
Rabbit monoclonal anti-Rab8	Cell Signaling Technology	Cat#6975S [D22D8]
Rabbit monoclonal anti-Rab11	Thermo Fisher Scientific	Cat#700184 [3H18L5]
Chemicals, Peptides, and Recombinant Proteins		
Osmium Tetroxide (4% solution)	Electron Microscopy Sciences	Cat#RT 19140
Protein G–Sepharose resin	BioVision Inc.	Cat#6511-5
DPX	Millipore Sigma	Cat#06522
L-α-phosphatidylinositol (Liver, Bovine) (sodium salt) (PI)	Avanti Polar Lipids	Cat#840042
1,2-dioleoyl-*sn*-glycero-3-phospho-L-serine (sodium salt) (DOPS)	Avanti Polar Lipids	Cat#840035C
1,2-Dioleoyl-sn-glycero-3-phosphocholine (DOPC)	Echelon Biosciences	Cat#L-1182
DiR';DiIC$_{18}$(7) (1,1'-Dioctadecyl-3,3,3′,3′-Tetramethylindotricarbocyanine Iodide)	Thermo Fisher Scientific	Cat#D12731
L-α-D-*myo*-Phosphatidylinositol 3-monophosphate, 3-O-phospho linked, D(+)-sn-1,2-di-O-hexadecanoylglyceryl (PI3P)	CellSignals Inc.	Cat#910
L-α-D-*myo*-Phosphatidylinositol 4-monophosphate, 3-O-phospho linked, D(+)-sn-1,2-di-O-hexadecanoylglyceryl (PI4P)	CellSignals Inc.	Cat#912
L-α-D-*myo*-Phosphatidylinositol 5-monophosphate, 3-O-phospho linked, D(+)-sn-1,2-di-O-hexadecanoylglyceryl (PI5P)	CellSignals Inc.	Cat#914
L-α-D-*myo*-Phosphatidylinositol 4,5-bisphosphate, 3-O-phospho linked, D(+)-sn-1,2-di-O-hexadecanoylglyceryl (PI(4,5)P_2)	CellSignals Inc.	Cat#902
L-α-D-*myo*-Phosphatidylinositol 3,4-bisphosphate, 3-O-phospho linked, D(+)-sn-1,2-di-O-hexadecanoylglyceryl (PI(3,4)P_2)	CellSignals Inc.	Cat#904
L-α-D-*myo*-Phosphatidylinositol 3,5-bisphosphate, 3-O-phospho linked, D(+)-sn-1,2-di-O-hexadecanoylglyceryl (PI(3,5)P_2)	CellSignals Inc.	Cat#906
L-α-D-*myo*-Phosphatidylinositol 3,4,5-trisphosphate, 3-O-phospho linked, D(+)-sn-1,2-di-O-hexadecanoylglyceryl (PI(3,4,5)P_3)	CellSignals Inc.	Cat#908

(*Continued on next page*)

Continued

REAGENT or RESOURCE	SOURCE	IDENTIFIER
Experimental Models: Cell Lines		
Human: Flp-In T-REx HeLa	Pietro De Camilli, Yale	N/A
Human: Flp-In T-REx HeLa GFP	This paper	N/A
Human: Flp-In T-REx HeLa GFP-PLEKHA4	This paper	N/A
Human: Flp-In T-REx HeLa PLEKHA4-GFP	This paper	N/A
Human: HEK293TN	Tony Bretscher, Cornell	N/A
Human: Flp-In HEK293	Pietro De Camilli, Yale	N/A
Human: Flp-In HEK293–GFP (SILAC Heavy/Light)	This paper	N/A
Human: Flp-In HEK293–GFP-PLEKHA4 (SILAC Heavy/Light)	This paper	N/A
Human: Flp-In HEK293–PLEKHA4-GFP (SILAC Heavy/Light)	This paper	N/A
Mouse: C57MG–WntRGreen	Anthony Brown, Weill Cornell Medicine (Santiago et al., 2012)	N/A
Mouse: MV7 Rat2a (control) MV7 Rat2a–Wnt1	Gerlinde Van De Walle, Cornell	N/A
Mouse: L (control) L–Wnt3a	Anthony Brown, Weill Cornell Medicine	N/A
Mouse: L–Wnt5a	ATCC	CRL-2814
Experimental Models: Organisms/Strains		
D. melanogaster: *y[1] M{w[+mC] = Act5C-Cas9.P}ZH-2A w[*]*	Bloomington Drosophila Stock Center	Stock# 54590
D. melanogaster: y^1 v^1 $P\{y^{+t7.7}$ *nos-phiC31\int.NLS};* *P{CaryP}attP40*	Bloomington Drosophila Stock Center	Stock# 25709
D. melanogaster: *y v; TM3, Sb / TM6B, Tb Hu*	This paper	N/A
D. melanogaster: *sp/CyoW (II); TM2/TM6B, Tb (III)*	This paper	N/A
D. melanogaster: *w[1] dsh[1]*	Bloomington Drosophila Stock Center	Stock# 5298
D. melanogaster: w[*] dsh[3] P{ry[+t7.2] = neoFRT}19A/FM7a	Bloomington Drosophila Stock Center	Stock# 6331
D. melanogaster: dsh[75] P{ry[+t7.2] = neoFRT}19A/FM7a	Bloomington Drosophila Stock Center	Stock# 68165
D. melanogaster: w[1118]; Df(3R)Exel6170, P{w[+mC] = XP-U}Exel6170/TM6B, Tb[1]	Bloomington Drosophila Stock Center	Stock# 7649
D. melanogaster: *pCasper4-Dsh-clover2*	Jeffrey Axelrod, Stanford	N/A
Oligonucleotides		
See Table S2 for oligonucleotide information		N/A
Recombinant DNA		
PLEKHA4 cDNA	DNASU	BC024157
pEGFP-C1	Clontech	Cat#6084-1
pEGFP-N1	Clontech	Cat#6085-1
mCherry-N1	Clontech	Cat#632523
mCherry-C1	Clontech	Cat#632524
GFP-PLEKHA4	This paper	N/A
PLEKHA4-GFP	This paper	N/A
mCherry-PLEKHA4	This paper	N/A
PLEKHA4-mCherry	This paper	N/A
GFP-PLEKHA4^{PH} (45–167)	This paper	N/A
GFP-PLEKHA4^{PRD} (167–357)	This paper	N/A
GFP-PLEKHA4$^{PRD\text{-}CC}$ (167–495)	This paper	N/A
GFP-PLEKHA4$^{PRD\text{-}CC\text{-}IDR}$ (167–779)	This paper	N/A
GFP-PLEKHA4^{CC} (357–495)	This paper	N/A
GFP-PLEKHA4$^{CC\text{-}IDR}$ (357–779)	This paper	N/A
GFP-PLEKHA4^{IDR} (495–779)	This paper	N/A
GFP-PLEKHA4$^{H\text{-}BP\text{-}PH}$ (28–167)	This paper	N/A
PLEKHA4$^{\Delta N+IDR}$ (28–495)-GFP	This paper	N/A
GFP-PLEKHA4$^{\Delta CC+IDR}$ (1–357)	This paper	N/A

(*Continued on next page*)

Continued

REAGENT or RESOURCE	SOURCE	IDENTIFIER
GFP-PLEKHA4$^{\Delta N+H+BP}$ (54–779)	This paper	N/A
GFP-PLEKHA4$^{\Delta PH}$ (1–45, 167–779)	This paper	N/A
GFP-PLEKHA4$^{\Delta H+BP+PH}$ (1–27, 168–779)	This paper	N/A
GFP-PLEKHA4$^{\Delta PRD}$ (1–167, 357–779)	This paper	N/A
GFP-PLEKHA4$^{\Delta IDR}$ (1–495)	This paper	N/A
pCDNA5-FRT	Thermo Fisher	Cat#K601002
pCDNA5-FRT-GFP-PLEKHA4	This paper	N/A
pCDNA5-FRT-PLEKHA4-GFP	This paper	N/A
pCDNA5-FRT-GFP	This paper	N/A
pcDNA3.1+zeo-VSV-KLHL12	Addgene	Cat#16761
pCMV10-3xFLAG	Sigma	Cat#E7658
3xFLAG-KLHL12	This paper	N/A
GFP-KLHL12	This paper	N/A
mCherry-KLHL12	This paper	N/A
pCMV-HA-N	Clontech	Cat#635690
CUL3 ORF	ORFeome8.1 library (Haiyuan Yu, Cornell University)	N/A
HA-CUL3	This paper	N/A
HA-Ub	Pietro De Camilli, Yale	N/A
M1R-mCherry	Pietro De Camilli, Yale	N/A
iRFP-PLCδ1-PH	Pietro De Camilli, Yale	N/A
mCherry-CRY2(PHR)	(Idevall-Hagren et al., 2012) Pietro De Camilli, Yale	N/A
mCherry-CRY2-PLEKHA4^{IDR}	This paper	N/A
mCherry-CRY2-PLEKHA4^{CC-IDR}	This paper	N/A
GFP-PLEKHA4^{PH} R75A	This paper	N/A
GFP-PLEKHA4^{PH} R129A	This paper	N/A
GST-PLEKHA4^{PH} R75A	This paper	N/A
GST-PLEKHA4^{PH} R129A	This paper	N/A
PLEKHA4$^{H-BP-PH}$-GFP	This paper	N/A
PLEKHA4$^{H-BP-PH}$-GFP F40E	This paper	N/A
PLEKHA4$^{H-BP-PH}$-GFP R75A	This paper	N/A
PLEKHA4$^{H-BP-PH}$-GFP R129A	This paper	N/A
PLEKHA4$^{H-BP-PH}$-GFP K42A/R43A/R48A/R49A (4A)	This paper	N/A
GST-PLEKHA4$^{H-BP-PH}$	This paper	N/A
GST-PLEKHA4$^{H-BP-PH}$ F40E	This paper	N/A
GST-PLEKHA4$^{H-BP-PH}$ R75A	This paper	N/A
GST-PLEKHA4$^{H-BP-PH}$ R129A	This paper	N/A
GST-PLEKHA4$^{H-BP-PH}$ K42A/R43A/R48A/R49A (4A)	This paper	N/A
pcDNA3.1+zeo-VSV-KLHL12: Q405X	This paper	N/A
GFP-PLEKHA4 S103, I106, R107, D109, and G110 silent (siRNA resistant)	This paper	N/A
PLEKHA4-GFP S103, I106, R107, D109, and G110 silent (siRNA resistant)	This paper	N/A
Software and Algorithms		
Fiji (ImageJ)	Schindelin et al., 2012	https://imagej.net/Fiji
Zen Blue 2.3	Zeiss	N/A
Zen Black	Zeiss	N/A
BD Accuri C6	BD Biosciences	N/A

CONTACT FOR REAGENT AND RESOURCE SHARING

Further information and requests for resources and reagents should be directed to and will be fulfilled by the Lead Contact, Jeremy Baskin (jeremy.baskin@cornell.edu).

EXPERIMENTAL MODEL AND SUBJECT DETAILS

Cell culture

Flp-In T-REx HeLa (Thermo Fisher), Flp-In HEK293 (Thermo Fisher), C57MG WntRGreen (Anthony Brown), L, L Wnt-3a, and L Wnt-5a cells (ATCC) and HEK293TN cells (Anthony Bretscher) were cultured in Dulbecco's modified Eagle medium (DMEM, Corning) supplemented with 10% fetal bovine serum (FBS, Corning) and 1% penicillin/streptomycin (P/S, Corning) at 37°C in a 5% CO_2 atmosphere. HEK293 cell lines were also supplemented with 1% sodium pyruvate (Corning) in the media. MV7-Rat2a-Wnt1 (Wnt1-secreting) and MV7-Rat2a (control) were cultured in above-mentioned conditions but in low glucose (1 g/L) DMEM. Stable expression of GFP, GFP-PLEKHA4 or PLEKHA4-GFP was achieved by transfecting Flp-In T-REx HeLa or Flp-In HEK293 cells (Thermo Fisher) with flippase (pOG44, Thermo Fisher) and above-mentioned plasmids cloned in pCDNA5-FRT vector following the manufacturer's protocol (Thermo Fisher). Twenty-four h post transfection, cells were selected with 100 μg/mL hygromycin B (Sigma). Conditioned media (CM) from L, L Wnt-3a, and L Wnt-5a cells was harvested by collection of supernatant from cells grown for at least 48 h and that had achieved at least 80% confluence, followed by passage through a 0.2 μm filter and storage at 4°C until use. Cell lines were obtained and used without further authentication.

Drosophila melanogaster husbandry

Information on individual fly strains is provided in the Key Resources Table. Flies were reared at room temperature in density-controlled vials (60-100 embryos/vial) on standard yeast-glucose medium, for experiments at L3 larval or adult stages. For experiments at 30 h after puparium stage, flies were reared in an incubate at 25°C and collected at the appropriate stage. Where possible, experiments were performed on both male and female flies to avoid sex-specific effects. Due to lethality of alleles on the X chromosome, involving flies with FM7a-balanced chromosomes, only female flies from such crosses were used for further analysis.

METHOD DETAILS

Plasmids and cloning

A PLEKHA4 cDNA (obtained from DNASU, corresponding to BC024157) was cloned into the pEGFP-C1 and -N1 vectors (Clontech) using EcoRI and SalI to generate GFP-PLEKHA4 and PLEKHA4-GFP, respectively. The full-length proteins were subcloned into mCherry-C1 and -N1 vectors using EcoRI and SalI. Fragments and deletions of PLEKHA4 were subsequently generated by subcloning into these vectors using standard or overlap PCR-based methods, again with EcoRI and SalI. The amino acid sequences of the deletions/fragments are the following: PLEKHA4^{PH} (45–167), PLEKHA4^{PRD} (167–357), PLEKHA4^{PRD-CC} (167–495), PLEKHA4$^{PRD-CC-IDR}$ (167–779), PLEKHA4^{CC} (357–495), PLEKHA4^{CC-IDR} (357–779), PLEKHA4^{IDR} (495–779), PLEKHA4$^{H-BP-PH}$ (28–167), PLEKHA4$^{\Delta N+IDR}$ (28–495), PLEKHA4$^{\Delta CC+IDR}$ (1–357), PLEKHA4$^{\Delta N+H+BP}$ (54–779), PLEKHA4$^{\Delta PH}$ (1–45, 167–779), PLEKHA4$^{\Delta H+BP+PH}$ (1–27, 168–779), PLEKHA4$^{\Delta PRD}$ (1–167, 357–779), PLEKHA4$^{\Delta IDR}$ (1–495). For bacterial expression, N-terminal fusions to GST of PLEKHA4^{PH} and PLEKHA4$^{H-BP-PH}$ were generated by subcloning into the pGEX-6P-1 vector (GE Healthcare) using EcoRI and SalI.

For generation of stable HeLa or HEK293 cells, GFP-PLEKHA4, PLEKHA4-GFP, and GFP were subcloned into the pCDNA5-FRT vector (Thermo Fisher) using NheI and KpnI (GFP-PLEKHA4), NheI and NotI (PLEKHA4-GFP and GFP). mCherry-KLHL12, GFP-KLHL12 and 3xFLAG-KLHL12 were generated by subcloning pcDNA3.1+zeo-VSV-KLHL12 (Addgene # 16761) into mCherry-C1, pEGFP-C1 vector using KpnI and ApaI, and into pCMV10-3xFLAG (Sigma) using HindIII and NotI. HA-CUL3 was cloned into pCMV-HA-N vector using XhoI and NotI by amplifying the CUL3 ORF from the ORFeome8.1 library (corresponding to GenBank BC039598.1, a gift from Haiyuan Yu, Cornell University). HA-Ub, M1R-mCherry, and iRFP-PLCδ1-PH was a gift from the De Camilli lab (Yale University). For optoDroplet experiments, mCherry-CRY2-PLEKHA4^{IDR} and mCherry-CRY2-PLEKHA4^{CC-IDR} were generated by cloning of the relevant PLEKHA4 fragment into mCherry-CRY2(PHR) (Idevall-Hagren et al., 2012) (a gift from Pietro De Camilli) using PvuI and KpnI.

The following mutations were introduced by Quikchange site-directed mutagenesis (Agilent) followed by DpnI digestion of the parental DNA strand. GFP-PLEKHA4^{PH}, GST-PLEKHA4^{PH}, PLEKHA4$^{H-BP-PH}$-GFP, GST-PLEKHA4$^{H-BP-PH}$: F40E, 4A (K42A/R43A/R48A/R49A), R75A, R129A; pcDNA3.1+zeo-VSV-KLHL12: Q405X. For rescue experiments, siRNA-resistant GFP-PLEKHA4 or PLEKHA4-GFP were generated by performing silent mutations at the following codons S103, I106, R107, D109, and G110, which is within the siRNA target region. All constructs were verified by Sanger sequencing (Cornell University Biotechnology Resource Center Genomics Facility).

Transfection of plasmids and siRNAs

Plasmid transfections were performed using Lipofectamine 2000 (Thermo Fisher) according to the manufacturer's protocol but using Transfectagro (Corning) instead of Opti-MEM. Cells were incubated with transfection mix in Transfectagro supplemented with 10% FBS for 6–8 h, following by a change of media to regular growth media and analysis after 18–20 h.

DsiRNA duplexes were obtained from Integrated DNA Technologies. Transfections with siRNA were performed with the appropriate duplexes (see Key Resources Table) using Lipofectamine RNAiMAX (Thermo Fisher) following the manufacturer's protocol except using Transfectagro in place of Opti-MEM. Cells were incubated wit transfection mix in Transfectagro supplemented with 10% FBS for 12–16 h, followed by exchange with fresh media. NC1 (negative control 1, IDT) was used as the control siRNA duplex for all experiments. Forty-eight h post transfection, cells were subjected to analysis via western blot, microscopy or flow cytometry.

Confocal microscopy

Prior to transfections (24 h), cells were seeded on 35 mm glass-bottom MatTek (#1.5 thickness, MatTek Corporation) imaging dishes for live cell imaging or on 12 mm cover glass (#1.5 thickness, Fisherbrand) for fixed cell imaging by immunofluorescence. Live cells were imaged 24–30 h post transfection. For immunofluorescence, cells were fixed in 4% paraformaldehyde in 100 mM sodium phosphate buffer (81 mM Na_2HPO_4-$7H_2O$, 21 mM NaH_2PO_4 pH 7.4) for 20 min, rinsed three times with PBS, blocked and permeabilized with blocking buffer (5% BSA and 0.1% Triton-X in 1X PBS) for 30 min. Cells were treated with primary antibody in blocking buffer for 1 h, rinsed with wash buffer (0.1% Triton-X, 1X PBS), incubated with secondary antibody in blocking buffer for 1 h at room temperature, rinsed with wash buffer and then PBS, mounted on slides in ProLong Diamond Antifade with DAPI (Thermo Fisher), and incubated overnight at room temperature in dark before imaging. For long-term storage, slides were stored at 4°C.

Images were acquired on a Zeiss LSM 800 confocal laser scanning microscope equipped with Plan Apochromat objectives (20x 0.8 NA or 40x 1.4 NA), and two GaAsP PMT detectors. Solid-state lasers (405, 488, 561, and 640 nm) were used to excite blue, green, red and far-red fluorescence respectively. Live-cell time-series movies were acquired using definite focus. For opto-Droplet experiments, a brief 488 nm pulse was used for photoactivation at the indicated frame in the time series. For colocalization-based analysis, multicolor images were acquired using line-scanning mode. Super-resolution structured illumination microscopy (SR-SIM) was performed on a Zeiss Elyra Super Resolution Inverted Axio Observe.Z1 microscope equipped with 405, 488, 561 and 640 nm lasers, definite focus and a Piezo-Z stage insert for fast focusing. Images were acquired using Zeiss Zen Blue 2.3 (confocal), Zeiss Zen Black (SR-SIM) and analyzed using FIJI (Schindelin et al., 2012).

Immunoprecipitation and western blots

Cells were harvested (500 x g, 3 min), lysed in lysis buffer (150 mM NaCl, 1% NP-40, 0.25% sodium deoxycholate, 5 mM EDTA, 50 mM Tris pH 7.5), sonicated for 3-5 pulses at 10% intensity, and centrifuged for 10 min at 13000 x g. A fraction of the supernatant was saved, quantified using the BCA assay (Thermo Fisher), and normalized as input, and the remainder was immunoprecipitated by rotation at 4°C overnight using either anti-GFP-nanobody Sepharose (Chromotek), EZview anti-FLAG-M2, or EZview anti-HA resins (Sigma). For immunoprecipitation using the soluble DVL3 antibody, the sample was incubated with primary antibody for 1 h at 4°C with rotation, followed by rotation overnight at 4°C with Protein G Sepharose (BioVision). The resin was then centrifuged for 10 min at 1000 x g, washed three times with lysis buffer and analyzed by SDS-PAGE and western blot, with detection by chemiluminescence (using SuperSignal West Pico (Thermo) or Clarity (Bio-Rad)) or, as described below in detail, mass spectrometry-based proteomics.

SILAC labeling and mass spectrometry-based proteomics analysis

For quantitative proteomics analysis, Flp-In HEK293 cells stably expressing GFP, GFP-PLEKHA4, or PLEKHA4-GFP were cultured in SILAC DMEM media (Thermo 89985) supplemented with 10% dialyzed FBS (JR Scientific) and 1% P/S for at least 5 passages (approximately 2 weeks) to allow full labeling of cells before analysis. "Light" SILAC media contained arginine $^{12}C6$, $^{14}N2$ and lysine $^{12}C_6$, $^{14}N4$, while "heavy" SILAC media contained "heavy" lysine $^{13}C6$, $^{15}N2$ and "heavy" arginine $^{13}C6$, $^{15}N4$.

Cells were lysed and immunoprecipiated with anti-GFP-nanobody Sepharose as described above and processed for mass spectrometry as described (Bastos de Oliveira et al., 2015, 2018) Briefly, the resin was washed three times with lysis buffer before treatment with elution buffer (100 mM Tris pH 8.0, 1% SDS) by incubation at 65°C for 15 min with intermittent tapping. The samples were reduced (10 mM DTT for 15 min), alkylated (10 mM iodoacetamide, 50 mM Tris pH 8.0), and then the "heavy" and "light" solutions were mixed in a 1:1 ratio. The protein was then incubated on ice for 30 min, centrifuged (4700 x g, 10 min) and washed with a solution of 50% acetone, 49.9% methanol, 0.1% acetic acid. The pellet was air-dried and resuspended in urea/Tris solution (8 M urea, 50 mM Tris pH 8.0) and NaCl/Tris solution (150 mM NaCl, 50 mM Tris pH 8.0) in a ratio of 1:3 respectively. Proteins were digested at 37°C overnight on a nutator with Gold trypsin (1 mg/mL, Promega) and then acidified with 10% trifluoroacetic acid and 10% formic acid. Samples were stored at –80°C if not analyzed immediately.

The samples were then desalted using a C18 column (WAT0549-55) and dried on a speedvac. The samples were then resuspended in 80% acetonitrile and 1% formic acid followed by fractionation using Hydrophilic Interaction Chromatography (HILIC). HILIC fractions were dried and reconstituted in 0.1% trifluoroacetic acid and analyzed using a Q-Exactive Orbitrap. Database search and quantitation of heavy/light peptide isotope ratios were performed using Sorcerer as previously described (Bastos de Oliveira et al., 2015, 2018). A complete list of hits from these proteomics studies is provided in Table S1 and describes two different experiments. Experiment #1: PLEKHA4-GFP (Light), GFP (Heavy); Experiment #2: GFP-PLEKHA4 (Heavy), GFP (Light).

Protein expression and purification in *E. coli*

A single colony of *E. coli* BL21-pRosetta2 transformed with wild-type or mutant GST-PLEKHA4^{PH} or GST-PLEKHA4$^{H\text{-}BP\text{-}PH}$ was grown in terrific broth (TB) supplemented with potassium phosphate buffer (0.17 M monobasic potassium phosphate, 0.17 M dibasic potassium phosphate), ampicillin and chloramphenicol for 6–8 h at 37°C, 250 rpm until OD_{600} was between 2 and 3. The temperature was then shifted to 18°C for 1 h, expression was induced with 0.25 mM isopropylthio-β-galactosidase (IPTG), and cells were grown overnight for at least 18–20 h at 18°C, 250 rpm. Cells were harvested (2100 x g, 15 min, 4°C) and stored at –80°C until use.

Frozen cell pellets were thawed in bacterial lysis buffer (20 mM Tris pH 8, 500 mM NaCl, 5% glycerol, 10 mM β-mercaptoethanol and 0.1 mM phenylmethylsulfonyl fluoride), sonicated, and centrifuged at 16,500 x g for 30 min to clear the lysate. The supernatant was incubated with washed Glutathione Sepharose 4B resin (GE Healthcare) for 1–2 h under nutation at 4°C. Bound complex was washed 15–20 times with lysis buffer and incubated overnight with PreScission protease to cleave off the GST tags. Supernatant was concentrated in 3K Amicon concentrators (Millipore), quantified using a Bradford assay, and flash frozen for storage at –80°C until use.

Liposome co-sedimentation assays

Liposomes were prepared by mixing 5:94:1 mol% ratio of phosphoinositide species:dioleoylphosphatidylcholine (DOPC):DiR (to aid in visualization of liposomes following SDS-PAGE) in 18:1 chloroform:methanol. Control liposome were DOPC:DiR (99:1 ratio) and dioleoylphosphatidylserine (DOPS):DOPC:DiR (20:79:1 ratio). After mixing, lipids were vacuum-dried, rehydrated in 25 mM HEPES pH 7.4 and 125 mM potassium acetate and incubated overnight at 37°C. Liposomes were generated by extruding lipids through 400 nm membranes (Whatman) and stored at 4°C protecting from light. The final phosphoinositide concentration was 20–100 μM (2–10 mol%), and the total lipid concentration was 1 mM. Catalog numbers of the exact lipid species used are reported in the Key Resources Table.

Liposome pelleting assay was performed to assess the binding of purified PLEKHA4 constructs to varying concentrations of phosphoinositide species *in vitro*. To avoid using any aggregates, each aliquot of purified protein was centrifuged at 163,000 x g for 10 min at 4°C following thawing and then re-quantified prior to use. This protein (2 μg) was incubated with liposomes (500 μM), giving a total lipid:protein ratio of 150:1 (phosphoinositide species:protein of 15:1 for 10% phosphoinositide-containing liposomes) for 10 min at room temperature in the dark. The reaction mixture was centrifuged at 163,000 x g for 30 min at 4°C. Supernatant and pellet were separated, denatured in SDS sample buffer and analyzed via SDS-PAGE gel. Images were acquired and quantified using a ChemiDoc MP system (Bio-Rad).

PI(4,5)P_2 depletion assay

HeLa cells were co-transfected with plasmids encoding M1R-mCherry, iRFP-PLCδ1^{PH}, and either GFP-PLEKHA4^{FL} or GFP-PLEKHA4$^{H\text{-}BP\text{-}PH}$ as described in Figures S1B and S1C. Twenty-four h after transfection, live-cell time-series with 5 s intervals between each frame, using definite focus as described above. During the time series, oxotremorine-M (10 μM) was added to induce PI(4,5)P_2 depletion.

Western blot analysis of DVL levels

Overexpression

HeLa cells were co-transfected with 500 ng each of FLAG-hDVL3 and the combination of GFP, GFP-PLEKHA4 or pCDNA3-VSV-KLHL12 plasmids as described in Figure 4A. The total DNA amount was normalized to 2.5 μg using pCDNA3 empty vector. After 36 h of cell growth post-transfection, the cells were lysed, quantified, normalized and analyzed by western blot. Experiments were performed in biological replicates, and chemiluminescence measured and quantified using a ChemiDoc MP system.

Endogenous levels

SiRNA duplexes (50 nM) against PLEKHA4 or KLHL12 was performed on either HeLa (human) or C57MG WntRGreen (mouse) cells on a 6-well plate. Forty-eight h post RNAi, cells were harvested, analyzed by western blot and levels of DVL1, DVL2 and DVL3 were quantified. Reported quantifications are from at least three biological replicates.

Analysis of DVL3 ubiquitination

Overexpression

HeLa cells were co-transfected with the combination of plasmids as described in Figures 4A and 4B. After 36 h of cell growth post-transfection, the cells were lysed, quantified, immunoprecipitated using EZview α-FLAG resin and analyzed by western blot.

Endogenous

SiRNA-mediated knockdown was performed against PLEKHA4 or KLHL12 on 60 mm dishes. After 48 h of cell growth post-transfection, cells were lysed and immunoprecipitated using 1 μg DVL3 primary antibody per 800 μg of lysate following the immunoprecipitation protocol as described above. Samples were analyzed in biological replicates via western blot and quantified as described above.

Rescue of DVL3 levels by PLEKHA4 transfection

RNAi was performed as described in HeLa cells but with cells seeded on 35-mm MatTek imaging dishes. Thirty-six h after the RNAi transfection, NC1-treated cells were transfected with 2 μg of GFP plasmid, siPLEKHA4 treated cells were transfected, using Lipofectamine 2000, with 2 μg of a plasmid encoding either GFP or PLEKHA4-GFP bearing silent mutations to render it resistant

to siRNA (Figure 4E). After 24 h of cell growth after the plasmid transfection, cells were treated with Hoechst 33342 (Thermo Fisher) and imaged via confocal microscopy to assess the transfection efficiency (which, for these experiments, was determined to be 50%–70%). After imaging, cells were harvested and analyzed via western blot.

Western blot analysis of β-catenin dependent Axin2 levels

Endogenous levels

Appropriate siRNA duplexes (50 nM) against PLEKHA4 or KLHL12 were transfected into HeLa (human) or C57MG WntRGreen (mouse) cells on a 6-well plate. Cells were stimulated with Wnt3a conditioned media 24 h post transfection. Forty-eight h post RNAi, cells were harvested, analyzed by western blot and quantified for Axin2 levels. Reported quantifications are from at least three biological replicates.

Rescue of Axin2 levels by PLEKHA4 transfection

RNAi was performed as described in HeLa cells. Thirty-six h after the RNAi transfection, NC1-treated cells were transfected with 2 μg of GFP plasmid, siPLEKHA4 treated cells were transfected with 2 μg of a plasmid encoding either GFP or PLEKHA4-GFP bearing silent mutations to render it resistant to siRNA (Figure 5E). Eight h after the plasmid transfection, cells were stimulated with Wnt3a conditioned media for 24 h, and analyzed by western blot. Reported quantifications are from at least three biological replicates.

Western blot analysis of β-catenin independent p-JNK levels

SiRNA duplexes (50 nM) against PLEKHA4 was transfected into C57MG WntRGreen cells on a 6-well plate. Cells were stimulated with conditioned media from L cells (control) or L Wnt-5a cells 24 h post transfection. Forty-eight h post RNAi, cells were harvested, analyzed by western blot and p-JNK levels were quantified. Reported quantifications are from at least three biological replicates.

Fluorescent Wnt reporter assay

RNAi (50 nM) was performed on C57MG WntRGreen as described above. After Thirty-six h after the siRNA treatment, MV7-Rat2a-Wnt1 (Wnt1-secreting) or MV7-Rat2a (control) cells were co-cultured with knockdown sample dishes in a 10:1 ratio of C57MG WntRGreen cells to MV7-Rat2a cells) and incubated at 37°C, 5% CO_2 atmosphere for an additional 26–30 h. Cells were then analyzed in biological replicates via flow cytometry (BD Accuri C6) or treated with Hoechst 33342 and analyzed by confocal microscopy. Separate dishes treated in exactly the same way were harvested for western blot analysis.

Generation of kramer (kmr) knockout flies

Sequences encoding an sgRNA targeting a region near the beginning of *kramer* (FlyBase: *CG34383*) open reading frame were cloned into the vector pCFD3 (Addgene # 49410). The construct was integrated into an *attP* docking site on the *Drosophila* chromosome 2 by injection into the strain y^1 v^1 $P\{y^{+t7.7}$ *nos-phiC31\int.NLS}; P{CaryP}attP40* (Bloomington stock center line 25709). Injected animals were mated to *y v* flies, and progeny with wild-type eyes were selected.

To make *kmr* knockout flies, males with the integrated sgRNA construct were mated with females of genotype y^1 $M\{w^{+mC}$ *Act5C-Cas9.P}ZH-2A w** (Bloomington stock center line 54590). Male progeny expressing Cas9 and the sgRNA were crossed with *y v; TM3, Sb / TM6B, Tb Hu* females. Single male progeny with the *TM3* balancer were then crossed to the same double balancer stock. Male and female progeny of this latter cross with the *TM6B, Tb Hu* balancer were intercrossed, and generating animals homozygous for putative mutations in *kmr.* These lines were genotyped by sequencing of appropriate PCR products to verify the homozygous knockout of *kmr* gene. We isolated and sequenced two *kmr* alleles with frameshift mutations early in the coding sequence predicted to result in loss of function, kmr^1 and kmr^2. In kmr^1, a 1 bp deletion created a frameshift mutation starting at the 89th codon. In kmr^2, a 2 bp deletion created a frameshift mutation starting at the 88th codon. See Figure S4 for relevant genomic sequences around the deletions that were determined by Sanger sequencing. Both stocks behaved identically in all subsequent experiments, and the either of the kmr^1 and kmr^2 alleles may be referred to simply as kmr^-.

Generation of flies containing kmr$^-$ and other alleles

To examine possible phenotypes associated with heterozygosity, five simple heterozygote strains (kmr^+/kmr^1, kmr^+/kmr^2, dsh^+/dsh^1, dsh^+/dsh^3, and dsh^+/dsh^{75}) were generated by crossing either homozygous (kmr^1, kmr^2, and dsh^1) or balanced (dsh^3/*FM7a* or dsh^{75}/*FM7a*) strains each separately with w^{1118}. The six transheterozygote strains ($kmr^+/kmr^-;dsh^+/dsh^1$, $kmr^+/kmr^-;dsh^+/dsh^3$, and $kmr^+/kmr^-;dsh^+/dsh^{75}$ for both the kmr^1 and kmr^2 alleles) were generated by crossing the appropriate homozygous *kmr* strain with either dsh^1, dsh^3/*FM7a*, or dsh^{75}/*FM7a*. To control for possible maternal effects, each cross involving kmr^1, kmr^2, or dsh^1 was carried out in two ways by switching the males and females and collecting the appropriate F1-generation flies for analysis; the results were identical. For crosses involving dsh^3/*FM7a* and dsh^{75}/*FM7a*, only virgin female flies were used and non-*FM7a* F1-generation female flies were selected for further analysis.

To determine whether wing hair polarity effects are due to knockout of *kmr* as opposed to off-target effects, complementation testing was performed between kmr^- and the deletion fragment *Df(3R)6170* (abbreviated as *df*), a chromosomal deletion encompassing 23 genes including *kmr. kmr*$^-$ flies were crossed with *Df(3R)Exel6170 / TM6B,* Tb^1 (Bloomington stock 7649), and non-Tb flies (kmr^{df}/kmr^-) were selected for analysis.

For assessing Dsh protein levels in wing imaginal discs and loss of proximal-distal asymmetry in pupal wings 30 h after puparium formation, we utilized *dsh::Clover* flies (a gift from Jeffrey Axelrod, Stanford University), which were generated by replacing the EGFP in pCasper4-Dsh-EGFP (Axelrod, 2001) with the fluorescent protein Clover2 followed by creation of transgenic lines with insertions on the second and third chromosomes (BestGene Inc.). First, *dsh::Clover/dsh::Clover* virgins (with *dsh::Clover* on chromosome 2 because *kmr* is on chromosome 3) were crossed with *sp/CyoW (II); TM2/TM6B, Tb (III) males*. In the F1 generation *dsh::Clover/CyoW; +/ TM6B, Tb* flies were collected and then crossed with kmr^{-} flies. Finally, the *Tb* progeny of the previous cross (*dsh::Clover/+;* kmr^{-}*/TM6B*) were collected and mated with kmr^{-} flies, generating kmr^{-} flies with a single *dsh::Clover* allele (*dsh::Clover;* kmr^{-}). Control flies that were wild-type at the *kmr* locus and bearing a single *dsh::Clover* allele (*dsh::Clover*), were also generated.

Dissection and imaging of wing imaginal discs, pupal wings, and adult wings

Wing imaginal discs

Wing imaginal discs (WIDs) were dissected from individual L3 larvae as described (Spratford and Kumar, 2014), and WIDs were fixed in 4% paraformaldehyde for 30 min, washed three times with wash buffer (5% BSA, 0.1% Triton-X, 1X PBS) and twice with 1X PBS. Genomic DNA was extracted from the remaining unfixed tissues from each individual larva for genotyping. From each animal, one pair of fixed and washed WIDs were mounted with ProLong Diamond Antifade without DAPI (Thermo Fisher) on glass slides under 12 mm coverglass (Fisher Scientific), and the slides were incubated overnight at room temperature in the dark before imaging. For long term storage, slides were stored at 4°C. For quantification of fluorescence from the Dsh-Clover protein fusion in WIDs, orthogonal view images were generated from the images of larvae that showed Clover signals post-genotyping. Dsh-Clover localizes in the epithelial folds of the WIDs (shown in Figure 7A with arrow). Three integrated density values (independent of the area) were generated from each image, and background was subtracted to obtain corrected integrated densities. Image analysis was performed in a manner blinded with respect to the animals' genotypes.

Pupal wings

Pupal wings were dissected from individual 30 h post puparium formation (APF) pupa as described (Bolatto et al., 2017). From each animal, one pair of fixed and washed pupal wings was mounted with ProLong Diamond Antifade without DAPI (Thermo Fisher) on glass slides under 12 mm coverglass (Fisher Scientific), and the slides were incubated overnight at room temperature in the dark before imaging. For long term storage, slides were stored at 4°C. Wings were imaged by confocal fluorescence microscopy, and maximum intensity z-projection images were generated and assessed for extent of proximal-distal symmetry.

Adult wings

Wings of appropriate genotypes were dissected and mounted on glass slides with mounting media (3:1 ratio of DPX:xylenes), and the slides were dried overnight at 50°C. Mounted wings were imaged by widefield brightfield microscopy.

Scanning electron microscopy (SEM)

Adult flies of correct genotype were collected and fixed in 2% glutaraldehyde in 0.05 M cacodylate buffer pH 7.4 for 2 h at 4°C. The samples were rinsed with 0.05 M cacodylate buffer three times for 5 min each and post fixed in 1% OsO_4 (osmium tetroxide, EMS) for 1 h at 4°C. The samples were rinsed again with 0.05 M cacodylate buffer three times for 5 min each. Serial dehydration was performed in 25%, 50%, 70%, 95%, 100% ethanol for 20 min each and 100% for 24–48 h at 4°C. Samples were critical point dried using a BAL-TEC CPD 030, mounted on stubs, and sputter coated with gold:palladium. Image analysis was performed using Tescan Mira3 FE-SEM microscope. At least 12 individual flies per genotype for eyes and thorax tissues each were analyzed, and four representative images per genotype are provided, one in Figure 6 and three in Figures S6 and S7.

QUANTIFICATION AND STATISTICAL ANALYSIS

Statistics and reproducibility

All imaging figures show representative images from experiments performed in at least three biological replicates on different days. For all experiments involving quantification, significance was calculated using an unpaired two-tailed Student's t test with unequal variance. Statistical significance of $p < 0.05$ or lower is reported. In figures containing bar graphs, the number of biological replicates analyzed has been stated in the legend, the height of the bar is the mean, the error bars represent standard deviation, and each overlaid dot represents an individual biological replicate. In the boxplot shown in Figure 7B, the boxes represent the middle quartiles, with the line in the middle representing the median, and the whiskers denote the maximum and minimum values. Image analysis was performed in a blinded manner.

DATA AND SOFTWARE AVAILABILITY

Data availability statement

The authors declare that all data supporting the findings of this study are available within the paper and its supporting information files.